

Research Article

Biogenic Silica Derived From Sugarcane Bagasse as a Precursor Material for Unmodified SBA-15: Physicochemical Properties and Their Use in Biodiesel Production From Spent Oil

Tatum Matthews ,¹ Ntalane Sello Seroka ,^{1,2} and Lindiwe Khotseng ¹

¹Department of Chemistry, University of the Western Cape, Cape Town, South Africa

²Energy Centre, Council for Scientific and Industrial Research (CSIR), Pretoria, South Africa

Correspondence should be addressed to Ntalane Sello Seroka; 3754640@myuwc.ac.za and Lindiwe Khotseng; lkhotseng@uwc.ac.za

Received 3 June 2025; Revised 17 September 2025; Accepted 20 September 2025

Academic Editor: Arnab Biswas

Copyright © 2025 Tatum Matthews et al. International Journal of Chemical Engineering published by John Wiley & Sons Ltd. This is an open access article under the terms of the Creative Commons Attribution License, which permits use, distribution and reproduction in any medium, provided the original work is properly cited.

Sustainable energy production requires innovative approaches to decrease the dependence on nonrenewable resources and reduce environmental impacts. In this proof-of-concept study, we investigated green Santa Barbara Amorphous 15 (SBA-15) catalysts using sugarcane bagasse ash (SCBA) as a silica source and incorporating organic acids and bases to create an eco-friendly synthesis pathway. These catalysts were applied in the transesterification of waste sunflower oil (WSO) to produce biodiesel. Although the overall biodiesel yields were relatively low, peaking at 5.603% FAME with the L-cysteine-modified SBA-15 catalyst (Lcys-500), the main objective of this study was to establish the feasibility of employing green SBA-15 materials as effective catalysts, rather than to optimise reaction parameters or maximise yield. Catalyst characterisation was carried out using X-ray diffraction (XRD), Fourier transform infrared spectroscopy (FTIR), scanning electron microscopy with energy-dispersive X-ray spectroscopy (SEM-EDS), transmission electron microscopy (TEM) and thermogravimetric analysis (TGA), confirming that the green SBA-15 retained key structural properties of conventional SBA-15, including ordered mesoporosity (*p6mm* symmetry) and spherical morphology with some variation in pore structure and thermal behaviour. Gas chromatography–mass spectrometry (GC–MS) was employed solely for biodiesel product analysis. FTIR spectra of the biodiesel confirmed successful transesterification, as indicated by characteristic C=O and C–O stretching bands. However, issues such as solidification of the CA-500-derived biodiesel and the low yield from the OP-after calcination sample (0.178%) underscore the need for further refinement. Importantly, catalyst modification strategies, such as surface functionalisation or metal doping, were beyond the scope of this initial study. Overall, the results support the feasibility of producing functional mesoporous SBA-15 catalysts from agricultural waste through green chemistry approaches. This study lays the groundwork for the development of environmentally friendly silica-based catalysts, with future research focussed on surface functionalisation to improve catalytic performance ecologically.

Keywords: biodiesel production; green SBA-15; silica-based materials; sugarcane bagasse ash; transesterification

Summary

- Sustainable Catalyst Synthesis: Green SBA-15 was synthesised from sugarcane bagasse ash using organic acids and alkalis, offering a green alternative to conventional HCl–SBA-15.
- Catalytic Performance: The unmodified green SBA-15 was tested for biodiesel production from waste sunflower oil, demonstrating measurable conversion efficiency.

- Comparative Analysis: Green SBA-15 and HCl–SBA-15 showed comparable mesostructural features, supporting further optimisation.

1. Introduction

The transition towards sustainable energy solutions is driven by the urgent need to reduce fossil fuel dependence and alleviate the environmental impacts associated with their

extraction and use. Among numerous renewable energy sources, biofuels such as biodiesel have emerged as alternatives due to their ability to lower greenhouse gas (GHG) emissions and utilise renewable or waste-derived feedstocks. Biodiesel is biodegradable, has exhibited compatibility with existing diesel engines and can be synthesised from low-value materials such as waste sunflower oil (WSO), offering both environmental and economic advantages [1–4].

A critical aspect of effective biodiesel production lies in the development of robust, affordable and environmentally friendly heterogeneous catalysts. Mesoporous silica materials, such as Santa Barbara Amorphous-15 (SBA-15), have garnered significant attention in this regard due to their ordered pore structure, high surface area and thermal stability, as illustrated in Figure 1 [5, 6]. SBA-15, typically synthesised via polymer-templated sol-gel methods, features uniform hexagonal mesopores and $p6mm$ symmetry, making it highly suitable for catalytic applications. However, conventional SBA-15 synthesis relies on costly and hazardous chemicals such as tetraethyl orthosilicate (TEOS) and hydrochloric acid (HCl), posing environmental, safety and economic concerns that limit their sustainable application [7–10].

While SBA-15 has previously been synthesised from biomass-derived silica, including sugarcane bagasse ash (SCBA), most studies continue to rely on hazardous mineral acids (e.g., HCl) and alkalis (e.g., NaOH) during synthesis [11]. This work introduces several key innovations that advance the green chemistry of SBA-15 materials. Firstly, we employed organic acids (citric acid [CA]) and amino acids (L-cysteine) in place of mineral acids for SCBA pretreatment. This rarely explored route may influence pore formation via hydrogen bonding or thiol interactions. Secondly, we implemented tetrapropylammonium hydroxide (TPAH) as an alternative alkaline agent for one-pot (OP) SBA-15 synthesis from SCBA-derived silica, representing a novel approach not yet reported in literature. This dual substitution of acid and base with greener, less hazardous reagents reflects a significant step towards environmentally benign mesoporous silica production. Importantly, we also assessed the baseline catalytic behaviour of the unmodified SBA-15 materials, rather than focussing on functionalised or doped variants, to establish a proper green foundation for future catalyst development.

Building on these innovations, our study focussed on SCBA as a renewable silica source and explored how different green pretreatment agents—namely, L-cysteine, CA, and TPAH—could influence the mesostructure of SBA-15. SCBA, an abundant agro-industrial byproduct, contains a high percentage of amorphous silica, making it a promising feedstock for the green synthesis of mesoporous materials. In addition to replacing synthetic silica precursors, the substitution of hazardous reagents with organic acids and bio-based additives can further reduce the environmental impact of SBA-15 synthesis. For instance, amino acids such as L-cysteine hydrochloride monohydrate offer functional groups ($-SH$ and $-NH_2$) that can influence silica condensation and pore structure through hydrogen bonding or electrostatic interactions [12–15].

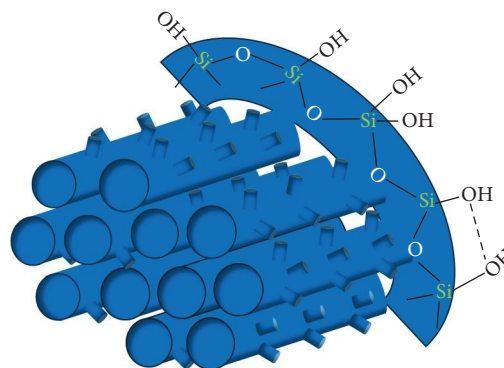


FIGURE 1: SBA-15 pore structure with silanol groups on its surface.

This study presents a proof-of-concept investigation into the green synthesis of SBA-15 using SCBA as a sustainable silica source and organic acids/bases as eco-friendly substitutes for conventional reagents. The goal is to evaluate the feasibility of producing mesoporous silica from waste materials under mild conditions and to assess the baseline catalytic potential of the unmodified materials in biodiesel production. Unlike many studies that apply postsynthesis functionalisation or doping to enhance catalytic performance, the present work deliberately focuses on raw, unmodified SBA-15 samples to understand their inherent structural, textural and catalytic properties. The establishment of the baseline characteristics is essential for future studies in catalyst optimisation and surface engineering.

For comparison, HCl-SBA-15 was synthesised and characterised to assess the structural and textural differences between green and conventional SBA-15. The samples were characterised using X-ray diffraction (XRD), Fourier transform infrared spectroscopy (FTIR), scanning electron microscopy with energy-dispersive X-ray spectroscopy (SEM-EDS), transmission electron microscopy (TEM), nitrogen physisorption (Brunauer–Emmett–Teller [BET]) and thermogravimetric analysis (TGA) to assess their structural and physicochemical properties. The materials were then tested as catalysts in the transesterification of WSO, with the resulting biodiesel products analysed using gas chromatography–mass spectrometry (GC–MS) and FTIR.

Although the biodiesel yields were relatively low, this outcome was expected and does not diminish the central purpose of the study, which was to demonstrate the viability of green SBA-15 synthesis using SCBA and to evaluate the potential of unmodified mesoporous silica as a foundational material for catalyst development. The results highlight the promise of biosilica-based SBA-15 as a green catalyst platform and lay the groundwork for subsequent research focussed on improving performance through functionalisation, doping, or acidity tuning.

Therefore, this research contributes to the growing field of renewable energy by illustrating the potential benefits of agricultural waste valorisation and catalyst development, paving the way for greener and more sustainable energy solutions.

2. Methods

2.1. Catalyst Preparation: Synthesis of SBA-15. The synthesis of SBA-15 catalysts was carried out using a templated sol-gel method, with a focus on green synthesis approaches incorporating organic acids and alkalis. The use of biomass-derived silica as a precursor offers a sustainable alternative to conventional methods that rely on synthetic silica sources [16]. This section details the synthesis procedures employed, including hydrothermal treatment, calcination conditions and modifications introduced to enhance the physico-chemical properties of the resulting SBA-15 catalysts.

2.1.1. Chemicals and Materials Used. The chemicals utilised in this study were L-cysteine hydrochloride monohydrate (98%), CA (98%) and pure water, which was used to wash the SCBA and remove soluble impurities. Sodium hydroxide (98%) and TPAH were employed to digest silica (SiO_2) from the SCBA to form sodium silicate (sol). Pluronic P123 and hydrochloric acid (32%) were used to produce the SBA-15 catalysts. Potassium hydroxide (99%), methanol (99%) and sulphuric acid (98%) were utilised in the transesterification of waste cooking oil (WCO) to biodiesel, along with the synthesised SBA-15. All chemicals used were analytical grade.

2.1.2. Feedstock Preparation. Sugarcane bagasse (SCB) feedstock was purchased from Sugar Illovo South Africa Company in KwaZulu-Natal. After collecting, the bagasse was allowed to air dry in the laboratory for approximately 7–14 days. Once completely dried, the SCB waste was collected, burnt in the open air, and reduced to ash; therefore, the remnants became the primary feedstock—SCBA. SCBA was then ground with a mortar and pestle until it was homogeneous before being filtered with a metal sieve to acquire a uniform particle size. The schematic overview of feedstock preparation is shown in Figure 2 [17–19].

2.1.3. Bagasse Pretreatment. To serve as a control sample in the comparison with green-synthesised SBA-15, HCl was employed for the acidic pretreatment of SCBA. The protocol outlined by Norsuraya [20] was followed. This involved weighing 5 g of raw SCBA and mixing it with 50 mL of a 1 M HCl solution in a round-bottom flask at room temperature for approximately 2 h, resulting in the production of HCl-treated SCBA (HCl-SCBA). Subsequently, the mixture was vacuum-filtered using a Buchner funnel, and the solid residue (HCl-SCBA) was washed with 20 mL of pure distilled water to eliminate any metallic ions. The HCl-SCBA was then dried in an oven set at 40°C for 24 h.

2.1.4. Sodium Silicate Extraction From the Bagasse. To synthesise sodium metasilicate (sodium silicate, Na_2SiO_3), alkali precipitation was employed to modify silica's physical and chemical properties and to eliminate any metal impurities. A 50 mL quantity of 3M sodium hydroxide (NaOH)

was required. To prepare this, 6 g of NaOH pellets were measured and combined with distilled water in a 50 mL volumetric flask. Following this, the HCl-SCBA sample (prepared earlier in section A) was introduced into the 3 M NaOH solution at 80°C and subjected to vigorous stirring for 4 h. Consequently, this process led to the development of an Na_2SiO_3 precipitate in the solution. This silica supernatant was subsequently used to manufacture SBA-15, referred to as HCl-SBA-15 (the control SBA-15 sample) [20, 21].

2.1.5. HCl-SBA-15 Catalyst Synthesis (Control). The SBA-15 catalyst was synthesised using silicate extracted from HCl-pretreated SCBA, as described in Section 2.1.4. A known quantity of Pluronic P123 was dissolved in deionised water under vigorous stirring at 40°C for 1 h. Next, 16 mL of the HCl-derived Na_2SiO_3 solution was added to the P123 solution and stirred continuously for an additional hour. Concentrated HCl was then introduced, and the mixture was stirred for 2 h.

The resulting gel was transferred to a Teflon-lined autoclave and subjected to hydrothermal ageing at 100°C for 48–62 h. The solid product was recovered by vacuum filtration, dried at 40°C for 12 h, and then calcined in a nitrogen atmosphere at 500°C for 1 h. The final control material is referred to as HCl-SBA-15.

2.1.6. Green SBA-15 Synthesis (CA-500 and Lcys-500). Green SBA-15 catalysts were synthesised using SCBA as the silica source, with CA and L-cysteine hydrochloride monohydrate (L-cys) used as environmentally friendly alternatives to conventional mineral acids. A modified version of the Norsuraya [20] method was adopted. SCBA was pretreated with CA or L-cys solutions under controlled conditions to leach impurities and liberate silica in a biodegradable medium. The sodium silicate (Na_2SiO_3) solutions used in this green synthesis were prepared using the same procedure outlined in Section 2.1.4, with the only modification being the substitution of CA or L-cys for HCl during SCBA pretreatment.

Initially, a specific quantity of Pluronic P123 copolymer was dissolved in a particular volume of deionised water in a glass container and stirred vigorously at 40°C for an hour to create a uniform P123/ H_2O solution. Next, 16 mL of CA and Lcys- Na_2SiO_3 was introduced to the P123/ H_2O solution. The mixture was stirred continuously at 40°C for an additional hour. Subsequently, a specified amount of concentrated HCl was added, and the mixture was stirred intensively for two more hours. The resulting gel was transferred to a Teflon-lined hydrothermal vessel and allowed to age at 100°C for 48–62 h under constant conditions. The cream-white solid that formed (SBA-15) was collected using vacuum filtration with a Buchner funnel and then dried in an oven for 12 h [22–24]. The dried substance underwent calcination in a tube furnace in a nitrogen atmosphere at 500°C for 1 hour. After the pyrolysis, the SBA-15/CA-500 and SBA-15/Lcys-500 catalysts were obtained and prepared for further evaluation.

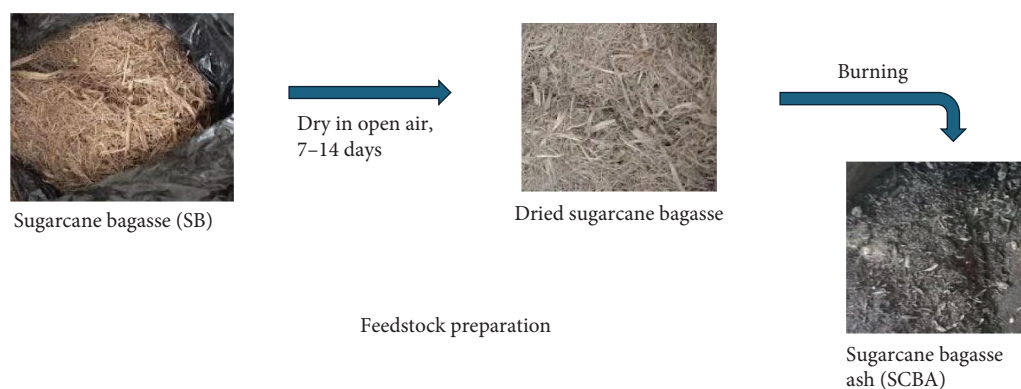


FIGURE 2: Schematic overview of feedstock preparation.

2.1.7. One-Pot SBA-15 Synthesis. For the first time, TPAH was employed as a novel alkaline agent in the synthesis of SBA-15 from biomass-derived silica, representing a green alternative to conventional methods. TPAH was used in place of sodium hydroxide (NaOH) to facilitate the formation of sodium metasilicate (Na_2SiO_3) from SCBA pretreated with L-cysteine (SCBA-Lcys) [25].

In a typical synthesis, a small quantity of SCBA-Lcys was mixed with TPAH solution in a round-bottom flask, yielding a viscous sludge. Simultaneously, Pluronic P123 was dissolved in deionised water under vigorous stirring for 1 h. Concentrated hydrochloric acid was then added to the SCBA-Lcys/TPAH mixture, followed by the gradual addition of the P123 solution. The final mixture was stirred for 2 h to ensure homogeneity.

The resulting gel underwent hydrothermal ageing at 100°C for 48–62 h. The solid product was filtered, washed and dried. To assess the impact of calcination, the dried material was divided into two portions: one was calcined under nitrogen at 500°C for 1 h (OP-A), and the other. At the same time, the other was left uncalcined (OP-B).

Calcination at 500°C was selected to remove residual organic matter and improve the purity and structural integrity of the silica framework. This step is critical for eliminating remnants from the biomass precursor and additives such as CA, L-cysteine and TPAH, while preserving the mesoporous architecture essential for catalytic activity. The treatment enhances surface area, thermal stability, and pore uniformity, making the material suitable for applications such as biodiesel production via transesterification.

Although the use of TPAH, CA, and L-cysteine does not eliminate environmental concerns, it reflects an advancement towards greener synthesis by replacing harsher reagents like NaOH and HCl with more manageable, less toxic alternatives. These reagents also offer potential for recovery and reuse in future scale-up processes.

2.2. Biodiesel Production and Analysis. Biodiesel was produced through the transesterification of WCO with the green-synthesised SBA-15 catalysts. The SBA-15 catalytic activity was assessed under predetermined reaction conditions, and the resulting biodiesel was analysed to determine its composition and quantity. Various analytical techniques,

including FTIR spectroscopy and GC-MS, were used to confirm the formation of biodiesel and evaluate its conversion efficiency [26, 27].

GC-MS was used to analyse the fatty acid methyl ester (FAME) composition of the generated biodiesel. The FAMES separation was accomplished with a capillary column, and components were identified by comparing retention times with known standards. This analysis provided insights into biodiesel composition, conversion efficiency and the catalytic performance of SBA-15 in the transesterification process [28, 29].

To the best of our knowledge, there is an evident lack of published studies examining the use of SBA-15 as the sole catalyst in simultaneous esterification and transesterification processes for WSO. This catalytic strategy represents a new and unexplored path in biodiesel production from WSO. We utilised the reaction parameters, such as reaction time, methanol-to-oil ratio, concentration and reaction temperature, identified as optimal for biodiesel production by Naser [30]. The optimal parameters are presented in Table 1.

The refined transesterification procedure, executed in a 500-mL round-bottom flask with a reflux condenser and a magnetic stirrer, implemented a meticulously arranged set of parameters [31]. Four distinct SBA-15 catalysts were employed: SBA-15/OP-B (one pot before), SBA-15/OP-A (one pot after), SBA-15/CA-500 and SBA-15/LCYS-500, respectively. The experiment commenced with magnetic stirring between 550 and 600 rpm to effectively mix the catalyst with methanol and p-WSO. Once the reaction was finalised, the catalyst was promptly separated from the product by means of a 30-min centrifugation at 6000 rpm. The mixture was then gently moved to a separating funnel, as depicted in Figure 3, and allowed to stand overnight to achieve the complete separation of biodiesel and glycerol [32, 33]. This thorough approach not only enhances the transesterification process but also ensures the creation of high-quality biodiesel suitable for detailed characterisation and evaluation.

2.3. Characterisation of Synthesised SBA-15

2.3.1. XRD. The materials' crystalline structures were examined using a Rigaku powder diffractometer, utilising

TABLE 1: The ideal parameters used in biodiesel production.

Parameter	Value
Reaction time	4 h
Methanol:oil ratio	1:8 mol/mol
Catalyst concentration	2% wt
Reaction temperature	65°C
RPM	550–600

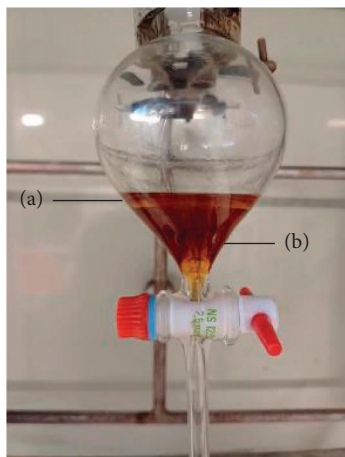


FIGURE 3: Successful (a) biodiesel layer and (b) glycerol layer in separating funnel produced from SBA-15-Lcys-500.

Cu-K α radiation ($\lambda = 1.54 \text{ \AA}$). Diffraction data were obtained at 2θ angles ranging from 5°C to 90°C at a scanning speed of $0.01^\circ\text{C}/\text{min}$ [34].

2.3.2. FTIR. The identification and composition analysis of the catalysts were examined with the Agilent 5500 compact FTIR spectrometer with Spectrum Two attenuated total reflectance (ATR), with a spectrum range of 400 and 4000 cm^{-1} and a resolution range of 2 to 16 cm^{-1} [35].

2.3.3. TGA. Material thermal stability was assessed through TGA using PerkinElmer's Simultaneous Thermal Analyzer, STA 8000. The experiments were conducted at ambient temperatures, ranging from 30°C to 800°C at a rate of $10^\circ\text{C}/\text{min}$, with cooling performed at $40^\circ\text{C}/\text{min}$ [36].

2.3.4. SEM-EDS. Scanning electron microscopy (SEM, TESCAN and VEGA), featuring a TESCAN dispersive X-ray spectrometer (EDS) operating at an accelerating voltage of 15 kV. SEM samples were produced on aluminium substrates and dried at 80°C for 1 h [37].

2.3.5. TEM Analysis. Examination of the surface and structural morphology of supplied materials was performed via TEM (JEOL, 2100), and the TEM samples were prepared by drop casting on copper grids and glass substrates, respectively. University of Cape Town, Electron Microscopic Unit (EMU) [38].

2.3.6. BET Analysis. Nitrogen-adsorption isotherm BET measurements were conducted using a MicroActive TriStar II 3020 instrument with the sample degassed under vacuum at 120°C for 24 h before analysis [39].

3. Results and Discussion

This section provides an in-depth evaluation of the green SBA-15 catalysts, CA-500, Lcys-500, OP-B and OP-A, synthesised using different pretreatment methods, and compares them with conventional SBA-15, specifically HCl-SBA-15. The novelty of this research lies in the green synthesis approaches, employing CA, L-cysteine hydrochloride monohydrate (Lcys), and TPAH as alternatives to the traditional HCl and NaOH pretreatment used in the production of SBA-15 from SCBA. These greener methods aim to reduce the environmental impact while maintaining or improving the catalytic efficiency of the material, especially for possible biodiesel production. The significance of this comparison stems from the need to explore more sustainable alternatives to conventional synthesis methods, aligning with the growing emphasis on green chemistry. The objective of this section is to examine the structural, textural and catalytic potential of these materials through various characterisation techniques like FTIR, XRD, SEM, TEM, BET and TGA to illustrate the structural integrity and porous nature of the SBA-15 samples. The catalytic performance of these materials in converting WSO to biodiesel will also be assessed. The resulting biodiesel was analysed using FTIR and GC-MS to evaluate its quality and conformity to biodiesel standards. Comparing the conventional HCl-SBA-15 with the green SBA-15 materials will provide valuable insights into the feasibility of adopting greener methods in heterogeneous catalysis for biodiesel production.

3.1. Characterisation Results of the SBA-15 Catalysts. The comparison of green SBA-15 with the established HCl-SBA-15 facilitates a thorough evaluation of the advantages and possible drawbacks of eco-friendly synthesis methods. The different SBA-15 catalysts are labelled as follows; see Table 2.

3.1.1. FTIR Spectroscopy Analysis. Attenuated total reflection Fourier transform infrared (ATR-FTIR) spectral analysis identified key functional groups existing in the SBA-15 samples, which were employed at room temperature with a wavelength range of $400\text{--}4000 \text{ cm}^{-1}$ and further validated the synthesis process of the different SBA-15 samples. Figure 4 shows the FTIR analysis of the prepared catalysts.

Analysis of the FTIR spectra of the mesoporous SBA-15 silica materials synthesised in Figure 4 and Table 3 reveals three distinct peaks, approximately at 480, 1084, and 700 cm^{-1} , corresponding to asymmetric and symmetric vibrations within the Si-O-Si network. The most prominent peaks occur in the $1100\text{--}1000 \text{ cm}^{-1}$ range, which corresponds to the asymmetric stretching vibrations of Si-O-Si bonds. This band is commonly associated with silica network formation, indicating that all samples exhibit a typical

TABLE 2: The sample name, treatment precursors and temperatures for the synthesised SBA-15 samples.

SBA-15 sample name	Pretreatment precursor	Alkali precursor	Temperature used (°C)
HCl-SBA-15	HCl	NaOH	500
CA-500	CA	NaOH	500
Lcys-500	L-cys	NaOH	500
OP-B (one pot before calcination)	L-cys	TPAH	500
OP-A (one pot after calcination)	L-cys	TPAH	500

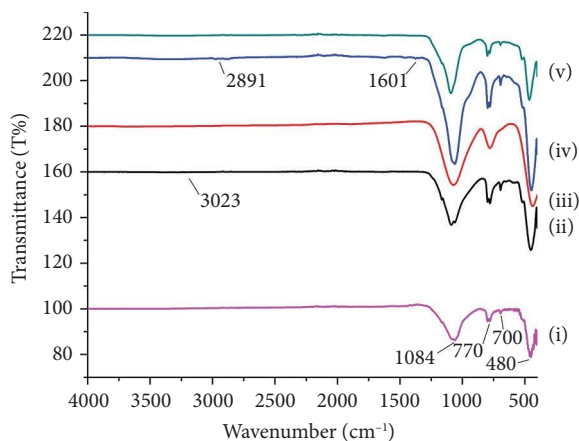


FIGURE 4: FTIR spectra of (i) HCl-SBA-15 (control sample), (ii) Lcys-500, (iii) CA-500, (iv) OP-B and (v) OP-A.

TABLE 3: Assignment of bands in the FTIR spectrum.

Wavenumber (cm ⁻¹)	Tentative band assignment
~480	Si-O-Si bending vibration
~700	Si-O-Si stretching vibration
~770	Si-OH vibration
~1084	Si-O-Si stretching vibration
1601	O-H band
2891	C-H stretch
3023	C-H stretch

SBA-15 structure. However, differences in the intensity and sharpness of these peaks suggest variations in the structural order of the silica, likely due to different synthesis or treatment conditions [40, 41].

HCl-SBA-15 showed well-defined Si-O-Si bands and no organic residues. Lcys-500 retained similar Si-O-Si features but exhibited C-H bands (~ 2900 cm⁻¹), indicating organic remnants. CA-500 lacked the ~ 700 cm⁻¹ band, suggesting possible structural alteration. OP-B exhibited pronounced C-H and O-H bands with intense Si-O-Si peaks, confirming organic content and a well-developed framework. After calcination, OP-A showed diminished organic bands and less intense Si-O-Si peaks, indicating partial framework restructuring [42, 43]. Therefore, the appearance of these peaks confirms the successful synthesis of mesoporous SBA-15 silicas [40, 44].

3.1.2. XRD Analysis. The XRD method was used to determine the characteristics of the crystalline phases by analysing the XRD angles from the crystalline phases of the SBA-15 catalysis.

The low-angle XRD pattern, Figure 5, of the HCl-SBA-15 sample shows well-defined peaks, including a strong (100) reflection near $2\theta = 0.3^\circ$, along with (110) and (200) reflections around 2θ values of 1.7° and 2° , confirming a highly ordered hexagonal mesoporous structure typical of SBA-15, with $p6mm$ symmetry. The sharpness and intensity of these peaks indicate uniform pore size distribution and a stable, regular arrangement of mesoporous [45, 46].

The low-angle XRD patterns of CA-500 and Lcys-500 are presented in Figure 6. It shows key structural differences in their mesoporous frameworks. Both catalysts show a prominent reflection (100) near 1° 2θ , confirming the retention of a hexagonal mesoporous structure typical of SBA-15. However, CA-500 shows smaller (100) and (200) peaks, indicating a well-preserved and uniform mesopore arrangement despite the CA treatment and calcination at 500°C . On the contrary, Lcys-500 lacks the (110) peak, suggesting a change in the order of the mesopores, likely due to the use of L-cysteine during synthesis. Lcys-500 also exhibits a broader and more prominent (200) peak compared to CA-500, which may indicate greater structural irregularities and enhanced scattering along the (200) plane. These differences suggest that, while both samples maintain a mesoporous structure, Lcys-500 has a less ordered arrangement, particularly along the (110) plane. A study by Dey and Samanta [47] illustrates the structural variations of SBA-15, such as the prominence of specific peaks, which synthesis conditions, calcination temperatures and treatments can influence. This supports our findings [47, 48].

The low-angle XRD patterns of OP-B and OP-A, as shown in Figure 7, reveal key differences in their structural ordering. Both samples display the (100), (110) and (200) peaks, indicating a well-ordered hexagonal mesoporous structure. However, OP-A shows a more pronounced (200) peak compared to OP-B, suggesting greater structural regularity along the (200) plane. While both samples retain long-range hexagonal ordering, the higher intensity of the (200) reflection in OP-A points to improved periodicity and possible differences in pore wall arrangement, making OP-A slightly more ordered than OP-B [49, 50].

Therefore, the low-angle XRD patterns of the green SBA-15 samples show distinct structural characteristics compared to those of HCl-SBA-15. The absence of significant peaks above 5° suggests that the samples are largely amorphous, with no crystalline silica phases. In general, XRD analysis confirms the successful synthesis of highly ordered mesoporous SBA-15 materials, further proven by the FTIR analysis above [51, 52]. The phase identification from the XRD spectra shows a similar trend to that of the study conducted by Medeiros [53].

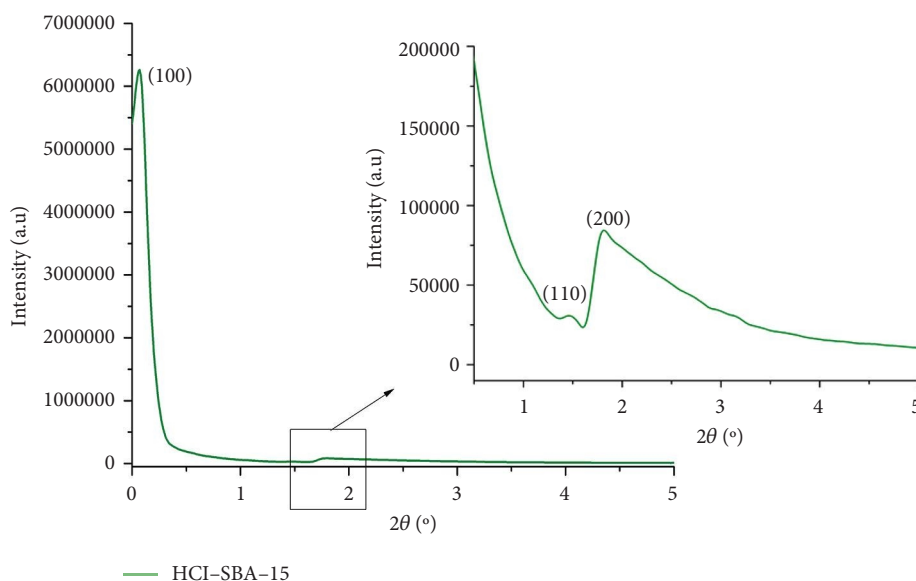


FIGURE 5: Low-angle XRD analysis of SBA-15 synthesised with HCl.

3.1.3. SEM-EDS Analysis. The SEM analysis reveals the morphological details of the catalysts' surface, while the EDS analysis provides information about the elemental composition of the catalysts. The surface morphology of the four different SBA-15 catalysts is depicted in the SEM images, Figure 8, at a magnification scale of 20 kx (10.4 μm).

SEM-EDS analysis was employed to investigate the morphological features and elemental composition of SBA-15 materials synthesised via both conventional and green methods. The traditional sample synthesised using hydrochloric acid (HCl-SBA-15) exhibited aggregated globular structures with rough surface textures, typical of well-developed mesoporous silica [54–56]. Elementally, it contained 9.41 wt% carbon, 58.91 wt% oxygen, 30.12 wt% silicon, and a minor fraction of aluminium at 1.57 wt%, indicating effective silica condensation with moderate removal of organic species. In comparison, the CA-derived sample calcined at 500°C (CA-500) presented more interconnected and smoother particles with reduced aggregation. Its composition—6.73 wt% carbon, 58.08 wt% oxygen and 35.19 wt% silicon—suggested improved silicate framework formation and efficient template removal. On the other hand, the L-cysteine-derived sample (Lcys-500) showed a notably different profile, with a highly porous and less compact morphology. EDS analysis revealed a significantly high carbon content of 48.83 wt%, alongside 42.56 wt% oxygen, 8.05 wt% silicon, and 0.56 wt% titanium, suggesting poor decomposition of the organic components during calcination and limited silica development. The significantly elevated carbon content observed in Lcys-500 is most likely due to the incomplete decomposition of L-cysteine residues during calcination. As an amino acid, L-cysteine contains functional groups such as $-\text{SH}$ and $-\text{NH}_2$ that can strongly interact with silica surfaces, potentially stabilising organic matter and impeding complete combustion under standard thermal conditions (500°C for 1 h). This suggests that the current calcination protocol may be insufficient to entirely remove residual organic species when amino acid-based pretreatment is employed. From a catalytic

perspective, the presence of excess carbon can block active mesoporous sites, reduce surface accessibility and interfere with acid site distribution—ultimately contributing to lower biodiesel yields. Interestingly, while L-cys-500 still achieved the highest FAME yield (5.6%), the residual carbon may have also introduced surface functionalities that enhanced oil-catalyst interactions. Future studies should consider thermal treatment optimisation or washing steps to remove residual organics while preserving beneficial surface chemistry [57, 58]. The presence of titanium, although minor, may stem from external contamination during synthesis or handling [59–61].

The OP synthesised sample before calcination (OP-before) showed dense, amorphous aggregates consistent with the retention of templating agents. Its elemental composition—33.47 wt% carbon, 54.06 wt% oxygen and 12.47 wt% silicon—reflected an early-stage mesostructure with unremoved organics. Following thermal treatment, the OP-after calcination sample exhibited improved particle definition and surface clarity, although EDS results indicated the persistence of residual carbon at 24.28 wt%. Oxygen and silicon were measured at 59.18 wt% and 16.08 wt%, respectively, with trace aluminium at 0.46 wt%. Despite calcination, the relatively high carbon level implies that the OP method may require further thermal optimisation to eliminate organic content. Among the green synthesis methods, the CA-500 sample demonstrated the most favourable elemental purity and silica network development. In contrast, the Lcys-500 and OP-after samples displayed residual organics that could influence their catalytic behaviour under reaction conditions [62, 63].

3.1.4. TEM Analysis. TEM analysis of the SBA-15 catalysts was performed to evaluate particle size and distribution, as shown in Figure 9. Figures 9(a), 9(b), 9(c), 9(d), and 9(e) were captured at a magnification of 50 nm, with specific regions of interest highlighted by red circles for further

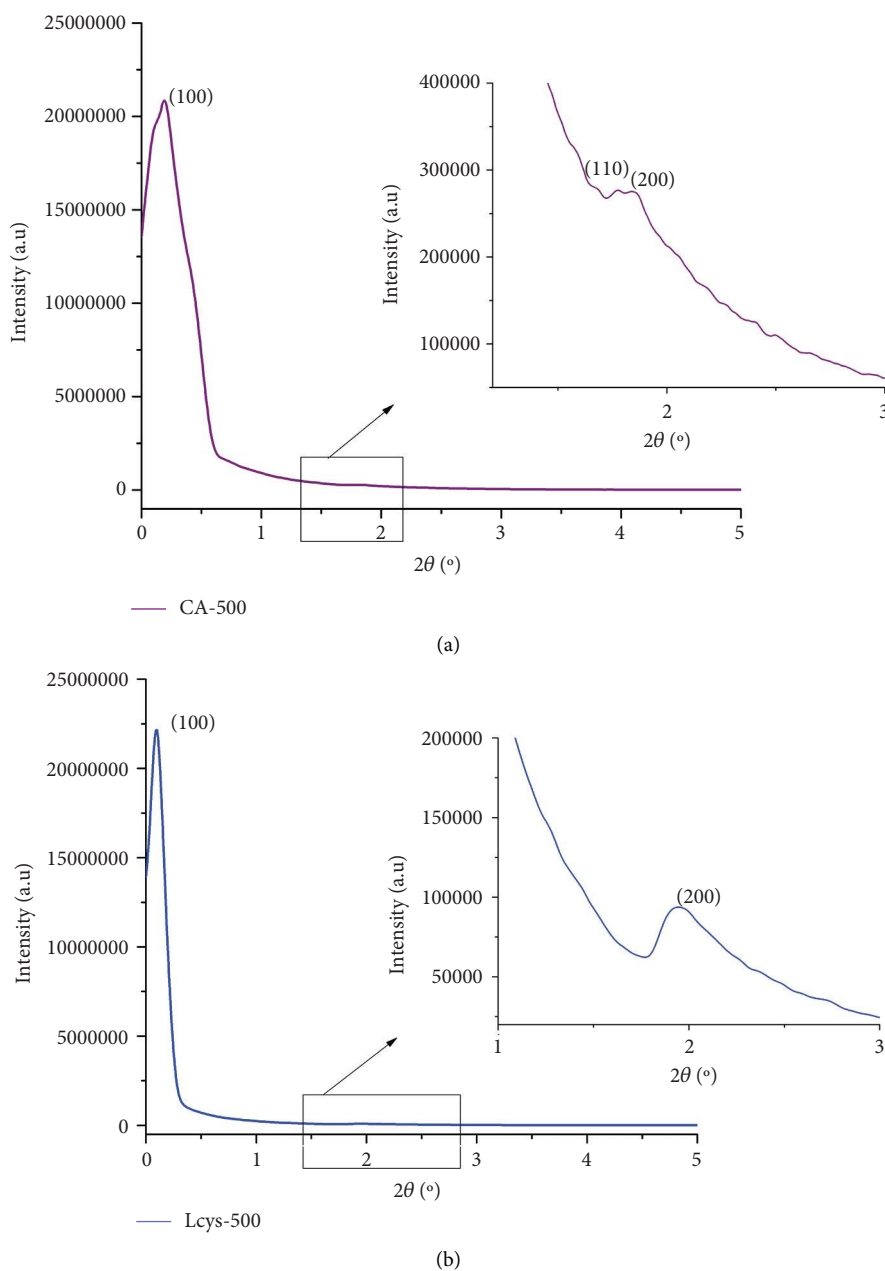


FIGURE 6: Low-angle XRD analysis of SBA-15 synthesised at 500°C with (a) CA and (b) L-cys.

detailed examination. The TEM images exhibit a characteristic hexagonal arrangement of uniform channels typical of SBA-15 materials [64, 65]. Postcalcination has a significant influence on particle size and distribution, as observed in the elongated, nonhomogeneous structures. These images underscore the critical role of calcination in shaping the final morphology and structural properties of the SBA-15 materials.

The TEM image of the HCl-SBA-15 (Figure 9(a)) sample reveals a typical mesoporous structure consistent with the characteristics of SBA-15 materials. In the region highlighted by the red circle, we observe a network of interconnected mesopores. The image shows some degree of agglomeration, but the individual pore walls are

relatively well-resolved. These mesopores are likely formed by the ordered hexagonal arrangement of silica, a characteristic of SBA-15 synthesised using hydrochloric acid as a catalyst. The scale bar indicates that the pore structures are in the nanometer range, with uniform channels that are typically observed in SBA-15. The contrast seen in the image suggests that the calcination process has successfully removed organic templates, resulting in clearer pores. However, the agglomeration observed may suggest slight structural deformation or incomplete removal of the template, which could affect the material's catalytic or adsorptive properties. Overall, the image confirms the presence of well-ordered, but possibly slightly disrupted, mesoporosity [66, 67].

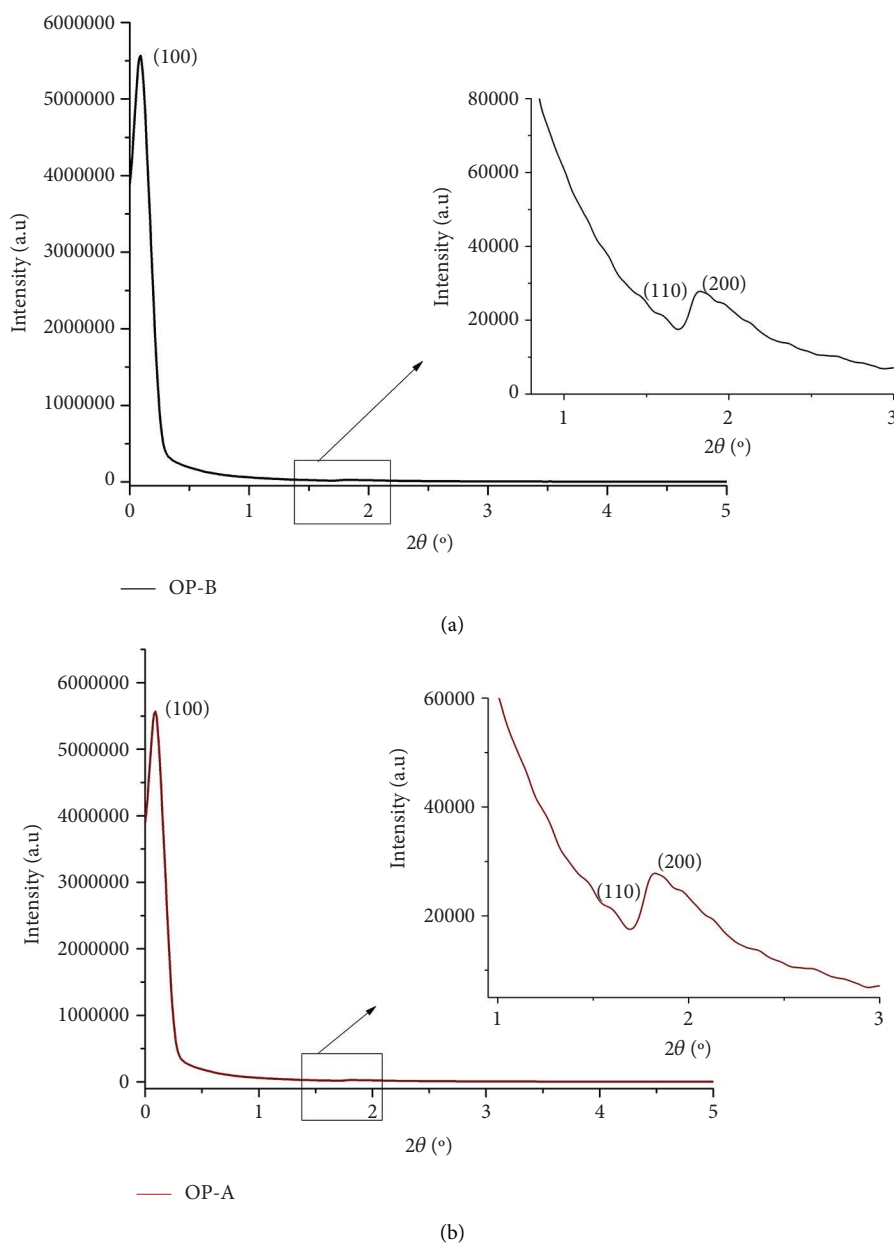


FIGURE 7: Low-angle XRD analysis of SBA-15 one-pot synthesis (a) before and (b) after calcination.

Figure 9(b), Lcys-500, shows a well-ordered, hexagonal arrangement of mesopores, typical of SBA-15 materials. The dark regions represent the silica walls, while the lighter areas represent the mesopores. The structure of this sample appears to retain its ordered porosity, indicating that L-cysteine did not interfere with the formation of mesopores. In Figure 9(c), the mesoporous structure appears loosely packed compared to Lcys-500. This could be attributed to the effect of CA, which may have influenced the formation of the mesoporous channels. The less-ordered arrangement indicates that the synthesis conditions may have been less favourable to achieve a highly ordered SBA-15 framework. However, the sample still retains the primary characteristics of SBA-15 [68]. The red circles in each image highlight fibre-like structures, characteristic of conventional

SBA-15 nanomaterials. As seen in Figure 9(b), there are cylindrical and spherical structures as well as thin, flaky composites with tiny dots (pores) in between, which may represent the walls of the mesopores within the SBA-15 materials. In Figure 9(c), note the presence of flaky and rod-shaped structures, as well as agglomerated particles (indicated by the dark areas throughout the TEM image), which form clusters and may be attributed to the alkaline pretreatment of the SCBA feedstock [65, 69].

Figure 9(d), OP-B, in this uncalcined sample, the mesoporous structure is not underdeveloped. For further analysis and discussion, in Figure 9(d), there appear to be multiple rod-like structures as well as some thin circular composites. There also appears to be an agglomeration of the particles, as indicated by the dark areas in the TEM image.

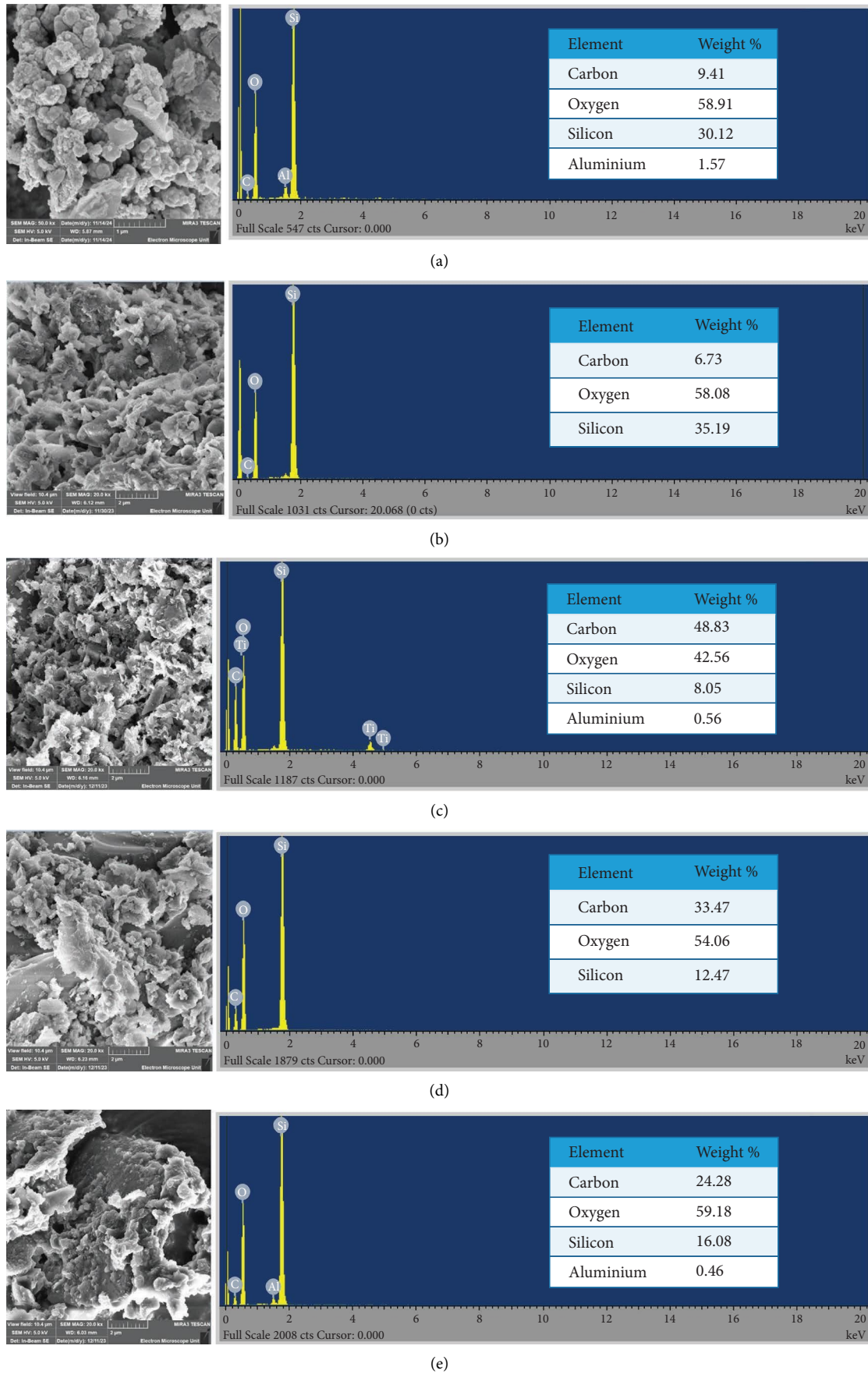


FIGURE 8: SEM-EDS images of (a) HCl-SBA-15, (b) CA-500, (c) Lcys-500, (d) OP-B and (e) OP-A.

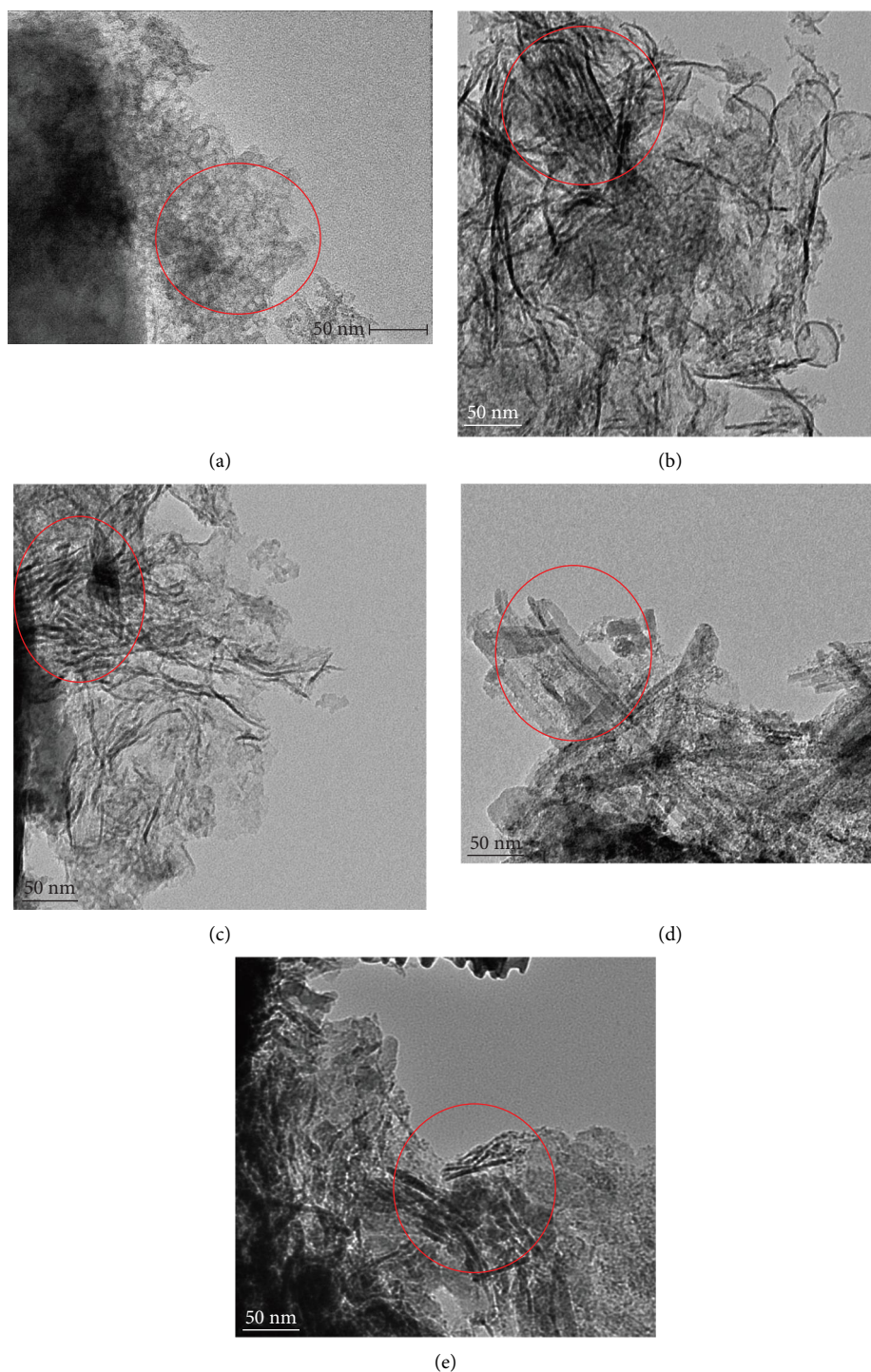


FIGURE 9: TEM images (a) HCl-SBA-15, (b) Lcys-500, (c) CA-500, (d) OP-B and (e) OP-A.

The pore structure appears disordered, and the framework is more amorphous in nature. This can be explained by the fact that the organic components (TPAH and L-cysteine) are still present, preventing the clear visualisation of the mesopores. The amorphous appearance suggests that the silica matrix has not fully formed its characteristic porous structure. Calcination is necessary to burn off the organic templates and reveal the ordered mesopores. In Figure 9(e), after

calcination, the OP synthesis sample exhibits a more defined mesoporous structure, although still not as ordered as the Lcys-500 sample. In Figure 9(e), after calcination, the OP synthesis sample exhibits a more defined mesoporous structure, though still not as ordered as the Lcys-500 sample. The pores are now visible, but their arrangement is less uniform compared to the other calcined samples—Figure 9(e) features fibre-like structures, as

highlighted and zoomed in. There are also thin, flaky composites and agglomerated particles, especially along the edge of the image. The use of TPAH and L-cysteine in the OP synthesis may have influenced pore formation, leading to a less organised mesoporous framework. However, calcination has improved the structural integrity of the material, and the pores are more prominent than in the uncalcined sample (OP-B) [69–71].

Therefore, in summary, HCl-SBA-15 exhibits a somewhat disordered structure, characterised by elongated particles and a certain degree of particle agglomeration. Compared to other samples, such as Lcys-500 and CA-500, which display more defined and uniformly packed mesoporous channels, HCl-SBA-15 appears less organised. The Lcys-500 sample exhibits better structural order, likely due to the presence of L-cysteine during synthesis. CA-500, while more ordered than HCl-SBA-15, still shows some particle elongation but has clearer mesoporous channels. On the other hand, OP-B and OP-A samples stand out with significantly more structured, plate-like arrangements and higher degrees of mesoporous channel alignment. OP-A demonstrates the most ordered structure, with rigid parallel channels, indicating that OP calcination-based synthesis helps maintain structural integrity more effectively than HCl-treated SBA-15. Overall, HCl-SBA-15 appears less ordered and uniform compared to the other samples, suggesting that the synthesis method greatly influences the structural properties of the final material. Furthermore, the TEM images agree with the SEM above regarding the visible agglomeration.

3.1.5. BET Analysis. BET surface area analysis is a widely used technique for determining the specific surface area of porous materials. The textural properties of the SBA-15 silicas were evaluated using the N₂ adsorption-desorption method, and the results are summarised in Table 4.

The BET isotherm plot (Figure 10) presents the nitrogen adsorption-desorption behaviour of various materials, indicating their pore structures and surface areas. The materials include HCl-SBA-15, CA-500, Lcys-500, OP-B and OP-A. The isotherms observed are Type IV, typical of mesoporous materials, which means they have pore sizes in the range of 2–50 nm. The presence of hysteresis loops at higher relative pressures suggests capillary condensation within the mesopores [72].

CA-500 exhibits the highest nitrogen adsorption capacity, reaching about 220 cm³/g, which suggests that this material has the largest surface area and pore volume among the samples. This significant adsorption capacity indicates a highly porous structure with a broad pore size distribution. In contrast, HCl-SBA-15 shows moderate adsorption, signifying a mesoporous material with a smaller surface area and pore volume than CA-500. Lcys-500, OP-B and OP-A exhibit much lower adsorption volumes, indicating that these materials have smaller surface areas and pore volumes. Among these, Lcys-500 shows the lowest adsorption, suggesting a significantly reduced porosity compared to the other samples [73, 74].

TABLE 4: Textural properties of the synthesised SBA-15 catalysts.

Sample name	BET _{SSA} (m ² /g)	V _P (cm ³ /g)	D _P (nm)
HCl-SBA-15	148.2910	0.37	4.8
Ca-500	220.368	0.32	15.6
Lcys-500	95.9744	0.44	14.9
OP-B	18.3384	0.09	4.5
OP-A	32.2193	0.08	4.7

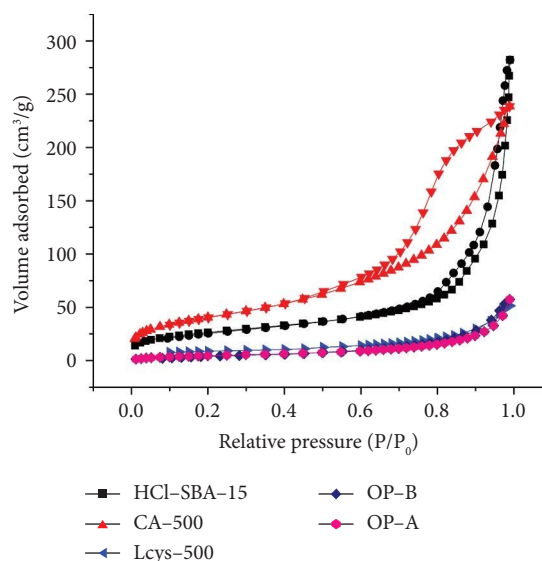


FIGURE 10: BET of the SBA-15 samples.

Most of the adsorption for these materials occurs within the relative pressure range of 0.6–1.0, which is consistent with the characteristics of mesoporous materials. The lower adsorption observed below P/P_0 of 0.6 for Lcys-500, OP-B and OP-A indicates minimal microporosity in these materials. The pronounced hysteresis loop for CA-500 further suggests the presence of ink-bottle-shaped pores. On the contrary, the less pronounced loops for the other materials may correspond to more uniform or cylindrical pore structures [75].

In summary, CA-500 has the highest porosity and surface area, followed by HCl-SBA-15, which has moderate properties. The remaining materials, Lcys-500, OP-B and OP-A, show significantly lower adsorption, indicating smaller pore volumes and less surface area.

3.1.6. TGA. TGA, as shown in the images, provides the weight loss of different SBA-15 samples as a function of temperature, offering insight into their thermal stability and the decomposition of organic or inorganic components [76]. The TGA graph in Figure 11 compares the thermal behaviour of five SBA-15 samples: HCl-SBA-15, CA-500, Lcys-500, OP-B and OP-A. The graph displays weight loss (%) as a function of temperature (°C) from 0°C to 600°C, revealing the thermal stability and decomposition profiles of these materials. TGA was used to assess the thermal stability of the catalysts over a specific temperature range.

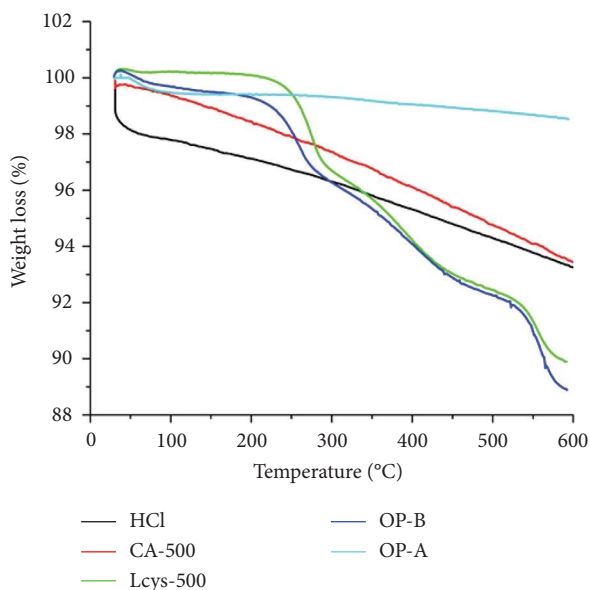


FIGURE 11: TGA distributions of the SBA-15 samples.

The TG analysis of the synthesised SBA-15 samples shows distinct mass decomposition steps. For HCl-SBA-15 (represented by the black curve), a smooth and gradual weight loss of approximately 3%–4% is observed, corresponding to the physically adsorbed water (30°C–100°C), the decay of the P123 template, and silanol decomposition (100°C–600°C), indicating the successful synthesis of SBA-15. This steady decrease in weight occurs without sharp transitions, illustrating the minimal presence of organic or moisture content within the material, confirming the overall high thermal stability of HCl-SBA-15 [77].

CA-500 analysis (represented by the red curve) reflects the minimal weight loss among all samples, indicating its exceptional thermal stability. Weight loss is gradual, occurring smoothly over the entire temperature range, with a total decline of approximately 2%–3%. This process exhibits similar decomposition steps to those of the HCl-SBA-15 sample. On the contrary, Lcys-500 (the green curve) exhibits two notable regions of weight loss. The initial loss, around 100°C, indicates the release of physically adsorbed water or volatile organic components. A more significant decline begins around 300°C and continues to 600°C, resulting in a total weight loss of approximately 7%–8%. This significant weight loss is likely attributed to the decomposition of cysteine residues from the functionalisation process, highlighting the organic content within the material [78, 79].

The thermal behaviour OP-B (represented by the blue curve) is characterised by multiple stages of weight loss, making it more complex than CA-500 and HCl-SBA-15. An initial minor weight loss at around 100°C is probably due to the release of water or light volatile organic components. This is followed by a sharp decline between 250°C and 450°C, associated with the decomposition of organic species, resulting in a total weight loss of approximately 6%. This pattern suggests that OP-B contains intermediate organic

content, possibly related to the synthesis or treatment employed. Lastly, OP-A (illustrated by the cyan curve) shows minimal weight loss, slightly higher than CA-500 but lower than L-cys-500 and OP-B. The weight loss is linear and gradual, amounting to around 3%, indicating that this material is also thermally stable with only small amounts of organic material. The TGA profile for OP-A is similar to CA-500; however, it exhibits a slightly higher overall weight loss, which may be due to minor residues or structural changes during the OP synthesis [79, 80].

The TGA data highlight the differences in thermal stability and organic content between the SBA-15 samples, relevant to their potential applications in catalysis or material science.

3.1.7. Comparative Summary of Catalyst Properties. To facilitate a more precise comparison of the structural and physicochemical features of the synthesised SBA-15 catalysts, a summary of key parameters is presented in Table 5. This includes surface area, pore diameter, pore volume (as determined by the BET method), carbon content (as measured by SEM-EDS), and thermal stability (as indicated by total weight loss from TGA).

This comparison illustrates the trade-offs between surface area, organic residue and thermal stability across different synthesis methods. Notably, CA-500 displayed the highest surface area and lowest thermal degradation, whereas Lcys-500 retained high porosity but showed substantial organic content. The OP samples (OP-B, OP-A) had significantly lower surface areas and higher carbon retention, correlating with their limited biodiesel yields.

3.2. Characterisation of the Biodiesel. The characterisation of the biodiesel produced in this study involves a comprehensive analysis of its physical and chemical properties to evaluate its quality and suitability as a biofuel. Analytical techniques, such as GC-MS, assess the content of FAME, viscosity, density and impurities, such as free fatty acids and water. Additionally, this analysis will help determine the catalytic effectiveness of SBA-15, especially evaluating whether SBA-15 alone can facilitate biodiesel production through transesterification or if further modifications/functionalisation are required to optimise the process. The reaction parameters of the transesterification process were 1: 8 oil-to-methanol ratio, 2% SBA-15 catalyst loading, at 60°C for 4 h.

3.2.1. FTIR Spectroscopy Analysis of the Biodiesel Samples. FTIR analysis of biodiesel samples produced using the green SBA-15 catalysts provides insight into the chemical composition and functional groups in biodiesel. When the vibrational frequencies are analysed, key functional groups, such as esters, can be identified, indicating successful transesterification. Characteristic absorption bands, such as the strong C=O stretching around 1740 cm⁻¹ and C-O stretching around 1020 cm⁻¹ range, are expected in biodiesel, confirming the formation of FAMES [81, 82].

TABLE 5: Summary of physicochemical properties of the SBA-15 catalysts.

Sample	Surface area (m ² /g)	Pore diameter (nm)	Pore volume (cm ³ /g)	Carbon content (wt%)	TGA weight loss (%)
HCl-SBA-15	148.29	4.8	0.37	9.41	~4
CA-500	220.37	15.6	0.32	6.73	~2–3
Lcys-500	95.97	14.9	0.44	48.83	~7–8
OP-B	18.34	4.5	0.09	33.47	~6
OP-A	32.22	4.7	0.08	24.28	~3

However, it must be noted that raw sunflower oil contains a C=O stretching band around 1740 cm⁻¹, thus it is not possible to rely solely on this band for determining successful biodiesel production. Therefore, the appearance of both 1740 cm⁻¹ (C=O) and 1020 cm⁻¹ (C–O) will indicate successful biodiesel production. This analysis is crucial in verifying the efficiency of the green SBA-15 catalysts in producing biodiesel and evaluating the purity and quality of the final product. This FTIR graph, Figure 12, shows the comparison of functional groups present in raw WSO and its biodiesel products (CA-500, Lcys-500, OP-B, OP-A), based on the wavenumber range from 4000 to 1000 cm⁻¹. Each curve represents the transmittance intensity at different wavenumbers, corresponding to specific chemical bond vibrations.

In Figure 12 and Table 6 [83], the WSO does not show significant peaks in 3000–4000 cm⁻¹, unlike the biodiesel samples (CA-500, Lcys-500, OP-B and OP-A), and this could be possible because the sunflower oil is expired. The FTIR spectrum for the WSO sample corresponds to a study conducted by Wembabazi et al. [84], in which expired sunflower oil was used to produce biodiesel [83]. Strong absorption peaks in the 3000–2800 cm⁻¹ region are characteristic of C–H stretching vibrations from alkyl groups (CH₂, CH₃), indicating the presence of triglycerides. In the range of 1700–1800 cm⁻¹, the peak corresponds to C=O stretching vibrations, typical of ester or carboxylic acid groups found in triglycerides. The 1200–1100 cm⁻¹ region reflects the C–H stretching vibrations in triglycerides [84, 85].

For the biodiesel samples, the 3500 cm⁻¹ region shows peaks (O–H stretch) that could be attributed to residual moisture from alcohols, as seen in Table 6. The 3000–2800 cm⁻¹ region also exhibits C–H stretching vibrations of the methyl and methylene groups, although the peak intensities differ slightly from those of WSO. These variations suggest structural changes during the transesterification process. In the 1740 cm⁻¹ region, the C=O stretching vibrations shift (from 1743 cm⁻¹ in the SSO spectrum to 1741 cm⁻¹ in the biodiesel spectra) or change in intensity, as expected during the conversion of triglycerides into methyl esters (biodiesel). For example, CA-500 exhibits a slightly stronger intensity in this region, indicating a more efficient conversion. At the same time, OP-A has the lowest intensity, possibly signalling incomplete conversion or the presence of intermediates. The 1022 cm⁻¹ peak, corresponding to C–O stretching vibrations, remains prominent in all biodiesel samples and is absent from the WSO, therefore further clarifying the successful production of biodiesel via

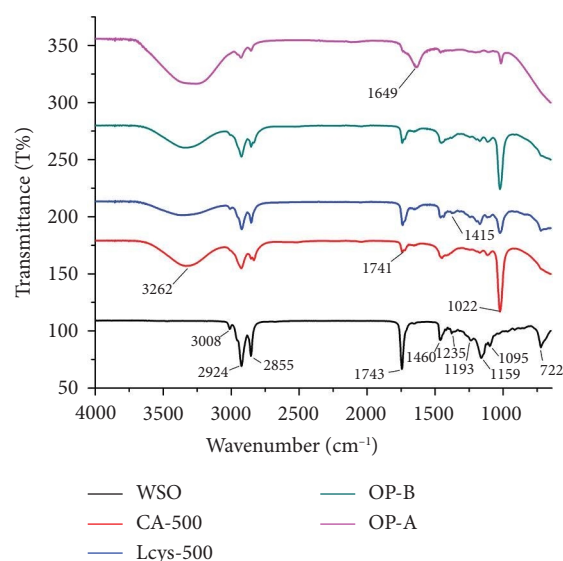


FIGURE 12: FTIR spectra of the WSO and the produced biodiesel samples.

TABLE 6: Wavenumbers and their corresponding bands.

Wavenumber (cm ⁻¹)	Groups attributed
3262	O–H broad stretch
3008	C–H stretch
2924	C–H stretch
2855	C–H stretch
1743	C=O stretch
1741	C=O stretch (ester)
1649	C=O stretch
1460	–CH ₂ in-plane bend (alkanes)
1415	C–H bend (alkanes)
1235	C–C bend
1193	C–C bend
1159	C–C bend
1095	C–O bend (alcohol, ester)
1022	C–O stretch (ester)
722	C–H bend (alkenes, long chain hydrocarbons)

transesterification with the SBA-15 catalysts. Although it varies in intensity and sharpness, reflecting differences in ester bonds formed during the reaction [86].

CA-500 and Lcys-500 both show clear and strong C=O (1741 cm⁻¹) and C–O peaks (1022 cm⁻¹), indicating efficient transesterification and the formation of ester bonds, typical of biodiesel. On the other hand, OP-B and OP-A display weaker C=O absorption, particularly OP-A, which suggests

incomplete conversion of triglycerides or the presence of unreacted oil. Additionally, the peaks near 3500 cm^{-1} in some biodiesel samples imply the presence of residual moisture or organic components, which could impact fuel quality. Furthermore, Lcys-500 has a medium peak near 3500 cm^{-1} , indicating that it contains less moisture/organic components, while the other samples have quite strong O–H peaks around 3500 cm^{-1} , meaning that they contain more moisture or residual organic components. Hence, this could affect the biodiesel production from the CA-500, OP-B and OP-A samples [81, 87].

In summary, the FTIR spectra indicate that the biodiesel samples have undergone successful transesterification, albeit with varying conversion efficiencies, as evidenced by differences in the ester C=O (1741 cm^{-1}) and C–O (1022 cm^{-1}) peaks. CA-500 and Lcys-500 appear to have the best conversion, while OP-A might need optimisation to improve its transesterification yield.

3.2.2. GC–MS Analysis. To evaluate the efficacy of the green-synthesised SBA-15 catalysts in producing biodiesel, GC–MS was used to analyse the FAME content of the biodiesel samples. The primary objective was to determine whether SBA-15 catalysts synthesised using green methods facilitated biodiesel production by converting the triglycerides in WSO into FAMES. GC–MS enables the separation and identification of individual components within the biodiesel, providing quantitative data on the relative abundance of different fatty acids [88]. This analysis is essential to understand the properties of the fuel, optimise the catalytic process, and confirm the potential of green SBA-15 as an effective catalyst in biodiesel production. The success of biodiesel production from WSO will be evaluated by examining four primary methyl esters illustrated in Table 7 [89].

3.2.2.1. FAME Analysis of Biodiesel Samples Using GC–MS. The biodiesel sample derived from the CA-500 catalyst, which was synthesised using CA, exhibited physical characteristics that hindered its analysis. Upon completion of the transesterification reaction, the CA-500 biodiesel solidified or hardened, making it impossible to undergo GC–MS analysis. The hardening of the biodiesel could be attributed to incomplete conversion, leading to residual unreacted triglycerides or glycerol, which can polymerise under certain conditions.

Another possible cause of solidification is the interaction between CA residues and methanol during the reaction. CA, being a tricarboxylic acid, can form complex esters or soaps under alkaline or acidic transesterification conditions. These products may lead to higher molecular weight species or increased viscosity, especially if the catalyst was insufficiently washed before use. Additionally, any residual moisture or improper separation of glycerol could have contributed to crystallisation. Furthermore, CA is soluble in methanol, so the solubility of CA could have affected biodiesel generation and resulted in its crystallisation [90, 91]. This observation highlights the potential challenges in using specific catalysts for biodiesel production, where the chemical conversion

TABLE 7: Methyl esters carbon chain and their corresponding names.

Methyl ester carbon chain	Methyl ester name
C16:0	Palmitate (palmitic acid)
C18:1	Oleate (oleic acid)
C18:2	Linoleate (linoleic acid)
C22:0	Docosanoic acid

must be carefully controlled and the physical properties of the final product must be closely monitored. In future work, thorough drying of the catalyst, improved postreaction washing and possibly adjusting the methanol-to-oil ratio may help prevent this phenomenon and improve the consistency of the biodiesel product.

As a result, only Lcys-500, OP-B and OP-A were subjected to GC–MS analysis. Table 8 displays the relative methyl esters detected in these three biodiesel samples. These esters are crucial indicators of biodiesel formation as they are FAMES derived from WSO.

For the Lcys-500 sample, high concentrations of palmitate (20.06 mg/g) and oleate (33.98 mg/g) were observed, the major components expected in SSO-based biodiesel. Linoleate (0.36 mg/g) and docosanoic acid (1.53 mg/g) were also detected, although in smaller amounts. The high levels of palmitate and oleate indicate that the Lcys-500 catalyst effectively produced biodiesel from SSO, successfully converting most of the fatty acids of sunflower oil into their methyl ester forms [91].

In the OP-B sample, palmitate (8.44 mg/g) and oleate (16.33 mg/g) were present, albeit at lower concentrations compared to Lcys-500, indicating that some biodiesel formation had occurred, although the conversion efficiency was lower. The concentration of linoleate (6.16 mg/g) was significantly higher than in Lcys-500, suggesting possible differences in reaction conditions or catalyst performance. A small amount of docosanoic acid (0.22 mg/g) was also detected. These data indicate that the OP-B sample achieved partial success in biodiesel production; however, the lower concentrations of key esters suggest an incomplete conversion of WSO [92, 93].

On the contrary, the OP-A sample contained small amounts of palmitate (1.78 mg/g), with oleate, linoleate and docosanoic acid not detected. The absence of significant concentrations of methyl ester indicates that OP-A was largely ineffective in producing biodiesel. The small number of palmitates suggests that the OP-A catalyst did not effectively convert WSO into biodiesel. In summary, the Lcys-500 sample demonstrated apparent success in the production of biodiesel from WSO, with high concentrations of palmitate and oleate indicating effective conversion. OP-B also produced biodiesel but with lower efficiency, as shown by reduced ester concentrations. OP-A, however, showed minimal biodiesel production, with insignificant levels of methyl esters, indicating that it was largely ineffective in converting SSO into biodiesel. Therefore, Lcys-500 was the most successful SBA-15 sample for biodiesel production, followed by OP-B, while OP-A showed limited success.

TABLE 8: Methyl ester concentrations in the biodiesel samples.

Methyl ester	Concentration in mg/g		
	Lcys-500	OP-B	OP-A
Palmitate	20.06	8.44	1.78
Oleate	33.98	16.33	0
Linoleate	0.36	6.16	0
Docosanoic acid	1.53	0.22	0

3.2.2.2. *Discussion of SBA-15 Catalyst Performance.* The GC-MS results indicate that the SBA-15 catalysts synthesised using green methods, particularly the L-cysteine-modified SBA-15 (Lcys-500), produced biodiesel, as evidenced by the presence of key FAMES. However, the overall FAME yield remained low across all samples, as seen in Figure 13 and Table 9. This suggests that while the green-synthesised SBA-15 catalysts can catalyse the transesterification of triglycerides into biodiesel, the process may require further optimisation to enhance reaction efficiency and recovery.

4. Summary

4.1. *Discussion on Synthesis of Green SBA-15.* In summary, FTIR analysis revealed distinct differences between the SBA-15 samples based on their synthesis and treatment methods. Sharp and well-defined Si-O-Si bands in HCl-SBA-15, CA-500 and OP-A demonstrated a successful formation of the mesoporous silica network, with minimal organic contamination after calcination. In contrast, OP-B showed significant organic residue, while the Lcys-500 sample exhibited intermediate characteristics. Regarding the XRD analysis, all green samples retained the characteristic peak (100) found in HCl-SBA-15, indicating that the mesoporous structure of SBA-15 was preserved. However, Lcys-500 lacked the (110) peak, although it had a prominent and broad (200) peak, suggesting some degree of structural order. On the other hand, CA-500, OP-B and OP-A exhibited both the (110) and (200) peaks, such as HCl-SBA-15, indicating a higher level of structural order. Quantitative elemental analysis as determined by SEM-EDS showed that all green SBA-15 samples contained Si, O and C. Lcys-500 had the highest carbon content (48%) and was hence considered the best green SBA-15 sample produced with OP-B being the second best and CA-500 the least favourable with 6% carbon content. Furthermore, the TEM provided the morphological information on the different SBA-15 silicas, and it was determined that OP-B and OP-A exhibited the best mesoporous structure, with Lcys-500 following. However, despite its structural ordering, OP-A exhibited inferior catalytic activity.

The poor catalytic activity of the OP-A sample can be attributed to multiple structural and chemical limitations. Despite showing improved mesopores ordering after calcination (as seen in the XRD and TEM analyses), the OP-A sample retained a relatively high carbon content (24.28 wt%) according to SEM-EDS results. This suggests that calcination may not have entirely removed organic residues from the OP synthesis, particularly TPAH and L-cysteine. These residuals could block active sites, reduce surface

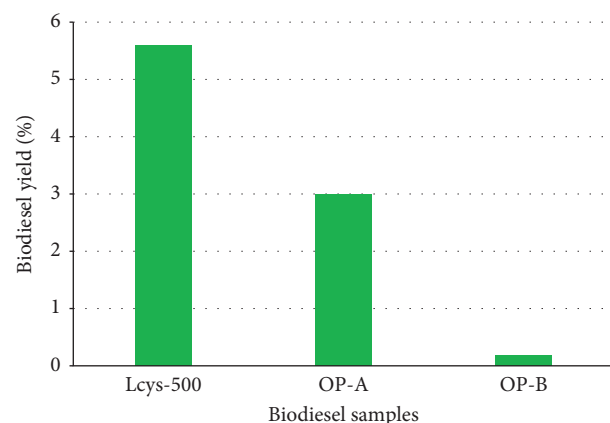


FIGURE 13: A bar graph illustrating the effect of the SBA-15 catalyst on the biodiesel yield.

TABLE 9: Biodiesel yield using green SBA-15 as a catalyst.

Sample name	Sample weight (g)	Biodiesel yield (%)
Lcys-500	0.0210	5.603
OP-B	0.0177	2.991
OP-A	0.0204	0.178

accessibility, or interfere with the adsorption of triglycerides. Moreover, the BET analysis indicated a very low surface area ($32.22 \text{ m}^2/\text{g}$) and limited pore volume, which severely restricts the available catalytic surface. This physical limitation, combined with incomplete template removal, likely suppressed transesterification activity. It is also possible that the interaction between TPAH and L-cysteine during OP synthesis created a denser silica framework with fewer acid sites or modified polarity, making it less compatible with oil-phase reactions. Future work should investigate optimising calcination time or temperature and explore the impact of post-treatment washing or mild functionalisation to restore active surface characteristics [94–97].

The BET results indicated that CA-500 and Lcys-500 showed significant increases in pore diameter and volume compared to the conventional HCl-SBA-15, suggesting that green synthesis methods can produce materials with enhanced porosity. The OP synthesised samples (OP-B and OP-A) displayed smaller pore sizes and volumes, indicating a more controlled mesoporous structure, though with potentially fewer surface areas for applications requiring a higher pore volume. Lastly, CA-500 and OP-A were the most thermally stable, with minimal degradation throughout the temperature range. Lcys-500 had the highest organic content, evidenced by its significant weight loss, while OP-B shows a moderate number of organic residues. HCl-SBA-15 exhibited good stability, albeit with a slightly higher overall weight loss compared to CA-500 and OP-A.

Therefore, as discussed above, the physical characteristics, thermal properties and quantitative elemental composition of the mesoporous SBA-15 silicas produced from SCBA have demonstrated that this study has successfully synthesised green SBA-15 with properties relatively similar to those of conventional HCl-SBA-15.

Although the acidity of the catalysts was not directly measured in this study, future work will involve quantitative characterisation using NH₃-TPD or pyridine-FTIR to better understand surface acid site density and its role in catalytic performance.

4.2. Discussion on Biodiesel Production With Green SBA-15 Catalysts. The FTIR spectra for the biodiesel samples revealed a shift in the C=O peak and the appearance of the C–O peak, indicating biodiesel production from WSO. From the characterisation of the green SBA-15 samples, the OP-after sample was expected to contain the highest FAME concentrations. Instead, it showed almost no detectable biodiesel (0.178%), raising questions about the reaction conditions or potential issues with the biodiesel extraction process. Furthermore, the solidification of the CA-500 biodiesel sample prevented its analysis, indicating possible complications with the catalyst or reaction conditions that resulted in the formation of a nonliquid product. These discrepancies underscore the importance of refining the catalytic process to ensure optimal conditions for biodiesel synthesis are met. Further studies could focus on modifying the catalyst structure, reaction temperature, and time to improve the biodiesel yield while also addressing any issues related to the physical properties of the final product.

In conclusion, while the SBA-15 catalysts demonstrated some capability to produce biodiesel, the GC–MS results suggest that the reaction was not entirely efficient under the tested conditions. More work is needed to fully assess the potential of these green-synthesised SBA-15 materials as catalysts for sustainable biodiesel production.

5. Conclusion and Future Recommendations

5.1. Conclusions. The primary aim of this study was to develop an eco-friendly method for synthesising SBA-15 using agricultural waste as a silica source, addressing environmental concerns associated with waste accumulation and the sustainability challenges of conventional, chemical-intensive SBA-15 synthesis. By focussing on the valorisation of biomass, this research successfully demonstrated the potential of agricultural waste to contribute to sustainable industrial practices and catalysis.

This research successfully demonstrated that SCBA, an abundant agricultural waste, can be effectively utilised as a renewable silica source for synthesising mesoporous SBA-15, resulting in the production of a novel material. By using SCBA, the research reduced reliance on hazardous chemicals commonly used in conventional SBA-15 synthesis, demonstrating a plausible approach to waste valorisation. An eco-friendly and straightforward synthesis method was developed, aligning with green chemistry principles, which highlights the environmental benefits of utilising biomass-derived silica. This sustainable approach addresses critical ecological challenges related to agricultural waste. It contributes to global sustainability efforts, particularly the

sustainable development goals (SDGs), by promoting clean energy, responsible resource management and climate action.

Characterisation techniques, including SEM and XRD, confirmed that the green-synthesised SBA-15 retained structural properties comparable to its conventional counterpart, including spherical particles and uniform hexagonal mesoporosity with *p6mm* symmetry. The green SBA-15 catalysts demonstrated the ability to produce biodiesel from WSO, with yields varying among the samples: Lcys-500 (5.6%), OP-B (2.99%) and OP-A (0.18%). Despite the low yields, the results validate that biodiesel production from WSO using green SBA-15 is feasible, though optimisation or functionalisation of the catalyst may enhance the efficiency and biodiesel yield.

The application of green SBA-15 in biodiesel production represents a dual waste utilisation strategy, addressing environmental pollution from agricultural residues and WSO while contributing to a circular economy. This approach aligns with SDGs 7 (affordable and clean energy), 11 (sustainable cities and communities) and 13 (climate action), reducing the environmental footprint of SBA-15 synthesis and advancing SDGs.

5.2. Future Recommendations. While this study provides insights into the synthesis of green SBA-15 and its application in biodiesel production, there remains considerable potential for further research and development in this field. Future work should focus on several key areas to enhance and expand the current findings.

Advanced characterisation techniques, such as single-crystal X-ray diffraction (SC-XRD), should be employed to provide more detailed insights into the crystalline structure and surface properties of the green SBA-15 material. Catalyst optimisation is another essential area for research, with a focus on improving the performance of green SBA-15. Investigating the influence of different synthesis conditions and material modifications, as well as evaluating the catalyst's stability and reusability, will be crucial for optimising its long-term performance in biodiesel production.

In addition to catalytic performance, further studies should assess the quality of the biodiesel produced using green SBA-15. Comprehensive testing of biodiesel quality, including parameters such as viscosity, density, flash point and cetane number, is needed to ensure the fuel meets established standards and regulatory requirements. Furthermore, optimising reaction parameters—beyond just the oil-to-methanol molar ratio—such as temperature, catalyst loading and reaction time, should be explored to maximise both biodiesel yield and quality.

In summary, this research highlights the feasibility and advantages of green SBA-15 synthesis and its application in biodiesel production. It underscores the importance of innovative strategies for waste management and sustainable energy, offering a scalable model with broader environmental and economic benefits.

Data Availability Statement

Data used are available in the article.

Conflicts of Interest

The authors declare no conflicts of interest.

Funding

This research was funded by the National Research Foundation (Grant no. 138079) and Eskom (South Africa) (Grant no. 2002/015527/0).

References

- [1] H. Saleh and A. Hassan, "The Challenges of Sustainable Energy Transition: A Focus on Renewable Energy," *Applied Chemical Engineering* 7, no. 2 (2024): 2084, <https://doi.org/10.59429/ace.v7i2.2084>.
- [2] R. El-Araby, "Biofuel Production: Exploring Renewable Energy Solutions for a Greener Future," *Biotechnology for Biofuels and Bioproducts* 17, no. 1 (2024): 129, <https://doi.org/10.1186/s13068-024-02571-9>.
- [3] M. A. I. Malik, S. Zeeshan, M. Khubaib, et al., "A Review of Major Trends, Opportunities, and Technical Challenges in Biodiesel Production From Waste Sources," *Energy Conversion and Management* (2024): 100675.
- [4] W. H. Foo, S. S. N. Koay, S. R. Chia, et al., "Recent Advances in the Conversion of Waste Cooking Oil Into Value-Added Products: A Review," *Fuel* 324 (2022): 124539, <https://doi.org/10.1016/j.fuel.2022.124539>.
- [5] P. Fulvio, S. Pikus, and M. Jaroniec, "Short-Time Synthesis of SBA-15 Using Various Silica Sources," *Journal of Colloid and Interface Science* 287, no. 2 (2005): 717–720, <https://doi.org/10.1016/j.jcis.2005.02.045>.
- [6] M. Zienkiewicz-Strzałka, S. Pikus, A. Deryło-Marczewska, and M. Błachnio, *Noble Metal Nanoparticles in Mesoporous Ordered Silica Systems* (2015).
- [7] W. Wang, J. Martin, X. Fan, A. Han, Z. Luo, and L. Sun, "Silica Nanoparticles and Frameworks From Rice Husk Biomass," *ACS Applied Materials and Interfaces* 4, no. 2 (2012): 977–981, <https://doi.org/10.1021/am201619u>.
- [8] W. Rehman, H. Wang, R. Manj, W. Luo, and J. Yang, "When Silicon Materials Meet Natural Sources: Opportunities and Challenges for Low-Cost Lithium Storage," *Small* 17, no. 9 (2021): 1904508, <https://doi.org/10.1002/smll.201904508>.
- [9] S. Prabha, D. Durgalakshmi, P. Aruna, and S. Ganesan, "Influence of the Parameters in the Preparation of Silica Nanoparticles From Biomass and Chemical Silica Precursors Towards Bioimaging Application," *Vacuum* 160 (2019): 181–188, <https://doi.org/10.1016/j.vacuum.2018.11.030>.
- [10] H. Li, X. Chen, D. Shen, F. Wu, R. Pleixats, and J. Pan, "Functionalized Silica Nanoparticles: Classification, Synthetic Approaches and Recent Advances in Adsorption Applications," *Nanoscale* 13, no. 38 (2021): 15998–16016, <https://doi.org/10.1039/d1nr04048k>.
- [11] V. Mamidi, R. Katakajwala, and S. V. Mohan, "Amorphous Nano-Silica From Sugarcane Bagasse Ash–Process Optimization, Characterization, and Sustainability Analysis," *Biomass Conversion and Biorefinery* 15, no. 3 (2025): 4059–4071, <https://doi.org/10.1007/s13399-024-05548-8>.
- [12] D. Mignogna, M. Szabó, P. Ceci, and P. Avino, "Biomass Energy and Biofuels: Perspective, Potentials, and Challenges in the Energy Transition," *Sustainability* 16, no. 16 (2024): 7036, <https://doi.org/10.3390/su16167036>.
- [13] M. Perišić, E. Barceló, K. Dimic-Misic, M. Imani, and V. Spasojević Brkić, "The Role of Bioeconomy in the Future Energy Scenario: A State-of-the-Art Review," *Sustainability* 14, no. 1 (2022): 560, <https://doi.org/10.3390/su14010560>.
- [14] H. Edelmann, N. Thieme, A. Ehrenreich, V. Zverlov, and W. Liebl, "Valorization of Milling Byproducts and Ergot-Sclerotia-Contaminated Rye Via Clostridial ABE Fermentation," *Biotechnology for Biofuels and Bioproducts* 17, no. 1 (2024): 139, <https://doi.org/10.1186/s13068-024-02590-6>.
- [15] Q. Li, Z. Wang, D. M. Fang, et al., "Preparation, Characterization, and Highly Effective Mercury Adsorption of L-Cysteine-Functionalized Mesoporous Silica," *New Journal of Chemistry* 38, no. 1 (2014): 248–254, <https://doi.org/10.1039/c3nj00799e>.
- [16] G. Ramalingam, A. K. Priya, L. Gnanasekaran, S. Rajendran, and T. K. Hoang, "Biomass and Waste Derived Silica, Activated Carbon and Ammonia-Based Materials for Energy-Related Applications—A Review," *Fuel* 355 (2024): 129490, <https://doi.org/10.1016/j.fuel.2023.129490>.
- [17] T. Wong, M. R. Mohd Hasan, and L. Peng, "Recent Development, Utilization, Treatment and Performance of Solid Wastes Additives in Asphaltic Concrete Worldwide: A Review," *Journal of Traffic and Transportation Engineering* 9, no. 5 (2022): 693–724, <https://doi.org/10.1016/j.jtte.2022.06.003>.
- [18] L. September, N. Kheswa, N. Seroka, and L. Khotseng, "Green Synthesis of Silica and Silicon From Agricultural Residue Sugarcane Bagasse Ash—A Mini Review," *RSC Advances* 13, no. 2 (2023): 1370–1380, <https://doi.org/10.1039/d2ra07490g>.
- [19] M. Amin, M. Attia, I. Agwa, Y. Elsakhawy, K. A. el-hassan, and B. Abdelsalam, "Effects of Sugarcane Bagasse Ash and Nano Eggshell Powder on High-Strength Concrete Properties," *Case Studies in Construction Materials* 17 (2022): e01528, <https://doi.org/10.1016/j.cscm.2022.e01528>.
- [20] S. Norsuraya, H. Fazlena, and R. Norhasyimi, "Sugarcane Bagasse as a Renewable Source of Silica to Synthesize Santa Barbara Amorphous-15 (SBA-15)," *Procedia Engineering* 148 (2016): 839–846, <https://doi.org/10.1016/j.proeng.2016.06.627>.
- [21] N. Rahmat, F. Hamzah, N. Sahiron, M. Mazlan, and M. Zahari, "Sodium Silicate as Source of Silica for Synthesis of Mesoporous SBA-15," in *IOP Conference Series: Materials Science and Engineering*, 133, no. 1 (IOP Publishing, June 2016), 012011, <https://doi.org/10.1088/1757-899x/133/1/012011>.
- [22] E. M. Björk, "Synthesizing and Characterizing Mesoporous Silica SBA-15: A Hands-On Laboratory Experiment for Undergraduates Using Various Instrumental Techniques," *Journal of Chemical Education* 94, no. 1 (2017): 91–94, <https://doi.org/10.1021/acs.jchemed.5b01033>.
- [23] A. L. Lázaro, F. J. Rodríguez-Valadez, J. J. M. López, and F. Espejel-Ayala, "SBA-15 Synthesis From Sodium Silicate Prepared With Sand and Sodium Hydroxide," *Materials Research Express* 7, no. 4 (2020): 045503, <https://doi.org/10.1088/2053-1591/ab83a5>.
- [24] P. Fulvio, S. Pikus, and M. Jaroniec, "Tailoring Properties of SBA-15 Materials by Controlling Conditions of Hydrothermal Synthesis," *Journal of Materials Chemistry* 15, no. 47 (2005): 5049–5053, <https://doi.org/10.1039/b511346f>.
- [25] A. Wassie and V. Srivastava, "Synthesis and Characterization of Nano-Silica From Teff Straw," *Journal of Nano Research* 46 (2017): 64–72, <https://doi.org/10.4028/www.scientific.net/jnanor.46.64>.

- [26] M. Mohiddin, Y. Tan, Y. Seow, et al., "Evaluation on Feedstock, Technologies, Catalyst and Reactor for Sustainable Biodiesel Production: A Review," *Journal of Industrial and Engineering Chemistry* 98 (2021): 60–81, <https://doi.org/10.1016/j.jiec.2021.03.036>.
- [27] D. Singh, D. Sharma, S. Soni, et al., "A Comprehensive Review of Biodiesel Production From Waste Cooking Oil and Its Use as Fuel in Compression Ignition Engines: 3rd Generation Cleaner Feedstock," *Journal of Cleaner Production* 307 (2021): 127299, <https://doi.org/10.1016/j.jclepro.2021.127299>.
- [28] C. Niemi, S. Lage, and F. G. Gentili, "Comparisons of Analysis of Fatty Acid Methyl Ester (FAME) of Microalgae by Chromatographic Techniques," *Algal Research* 39 (2019): 101449, <https://doi.org/10.1016/j.algal.2019.101449>.
- [29] A. C. B. Tercini, M. Pinesi, G. Cyntia Calera, et al., "Ultrafast Gas Chromatographic Method for Quantitative Determination of Total FAMES in Biodiesel: An Analysis of 90s," *Fuel* 222 (2018): 792–799, <https://doi.org/10.1016/j.fuel.2018.03.008>.
- [30] S. Naser, *Application of Graphenated Nano Zero Valent Iron in the Catalytic Conversion of Spent Vegetable Oil into Biodiesel* (University of the Western Cape, 2023).
- [31] V. Patil-Shinde, V. Lakshete, and S. Gadekar-Shinde, "Biodiesel Synthesis From Waste Sunflower Oil: Experimental and Multilayer Perceptron Neural Network Modeling," *Materials Today: Proceedings* (2023): <https://doi.org/10.1016/j.matpr.2023.01.117>.
- [32] J. Yang, Y. Feng, T. Zeng, et al., "Synthesis of Biodiesel Via Transesterification of Tung Oil Catalyzed by New Brønsted Acidic Ionic Liquid," *Chemical Engineering Research and Design* 117 (2017): 584–592, <https://doi.org/10.1016/j.cherd.2016.09.038>.
- [33] R. Ampairojanawong, A. Boripun, S. Ruankon, T. Suwanasri, K. Cheenkachorn, and T. Kangsadan, "Separation Process of Biodiesel-Product Mixture From Crude Glycerol and Other Contaminants Using Electrically Driven Separation Technique With AC High Voltage," *Electrochemistry* 4, no. 1 (2023): 123–144, <https://doi.org/10.3390/electrochem4010011>.
- [34] A. Llewellyn, A. Matruglio, D. Brett, R. Jarvis, and P. Shearing, "Using In-Situ Laboratory and Synchrotron-Based X-Ray Diffraction for Lithium-Ion Batteries Characterization: A Review on Recent Developments," *Condensed Matter* 5, no. 4 (2020): 75, <https://doi.org/10.3390/condmat5040075>.
- [35] M. Radebe and B. Wilhelm, "Development of Rheo-IR: Combination of a Strain-Controlled Rheometer With an IR Spectrometer for In-Situ Mechanical and Chemical Analysis of Cement Paste" (2022).
- [36] N. Zainal, J. Saiter, S. Halim, R. Lucas, and C. Chan, "Thermal Analysis: Basic Concept of Differential Scanning Calorimetry and Thermogravimetry for Beginners," *Chemistry Teacher International* 3, no. 2 (2021): 59–75, <https://doi.org/10.1515/cti-2020-0010>.
- [37] N. Erdman, D. Bell, and R. Reichelt, *Scanning Electron Microscopy* (Springer Handbook of Microscopy, 2019).
- [38] A. Gkoutzidou, "Transmission Electron Microscopy Imaging and Spectroscopy of 2D Materials for Biological Applications" (2020).
- [39] F. Fu, L. Lin, and E. Xu, "Functional Pretreatments of Natural Raw Materials," in *Advanced High Strength Natural Fibre Composites in Construction* (Woodhead Publishing, 2017), 87–114.
- [40] N. Rahmat, M. Sabali, A. Sandu, N. Sahiron, and I. G. Sandu, "Study of Calcination Temperature and Concentration of NaOH Effect on Crystallinity of Silica From Sugarcane Bagasse Ash (SCBA)," *Revue Chimique* 67 (2016): 1872–1875.
- [41] R. Dey, R. Gupta, and A. Samanta, "Carbon Dioxide Capture Under Postcombustion Conditions Using Amine-Functionalized SBA-15: Kinetics and Multicyclic Performance," *Separation Science and Technology* 53, no. 16 (2018): 2683–2694, <https://doi.org/10.1080/01496395.2018.1461114>.
- [42] R. Nechikkattu and C. Ha, "Tunable Catalytic Activity of Gold Nanoparticle Decorated SBA-15/PDMAEMA Hybrid System," *Journal of Porous Materials* 27, no. 2 (2020): 611–620, <https://doi.org/10.1007/s10934-019-00847-2>.
- [43] A. M. Thomas, J. Peter, S. Nagappan, A. Mohan, and C. Ha, "Dual Stimuli-Responsive Copper Nanoparticles Decorated SBA-15: A Highly Efficient Catalyst for the Oxidation of Alcohols in Water," *Nanomaterials* 10, no. 10 (2020): 2051, <https://doi.org/10.3390/nano10102051>.
- [44] S. Nasreen, U. Rafique, S. Ehrman, and M. Ashraf, "Synthesis and Characterization of Mesoporous Silica Nanoparticles for Environmental Remediation of Metals, PAHs and Phenols," *Ekoloji* 27, no. 106 (2018): 1625–1637.
- [45] S. Park, S. Chu, L. Shi, S. Yuan, and C. Ha, "SBA-15 With Crystalline Walls Produced Via Thermal Treatment With the Alkali and Alkali Earth Metal Ions," *Materials* 14, no. 18 (2021): 5270, <https://doi.org/10.3390/ma14185270>.
- [46] M. Oliveira, L. Bieseki, A. Alencar, T. Braga, and S. Pergher, "Incorporating Aluminum Into the Structure of SBA-15 by Adjusting the pH and Adding NaF," *Materials Research* 22, no. 3 (2019): e20180657, <https://doi.org/10.1590/1980-5373-mr-2018-0657>.
- [47] R. Dey and A. Samanta, "Microwave-Synthesized High-Performance Mesoporous SBA-15 Silica Materials for CO₂ Capture," *Korean Journal of Chemical Engineering* 37, no. 11 (2020): 1951–1962, <https://doi.org/10.1007/s11814-020-0596-0>.
- [48] P. Verma, Y. Kuwahara, K. Mori, R. Raja, and H. Yamashita, "Functionalized Mesoporous SBA-15 Silica: Recent Trends and Catalytic Applications," *Nanoscale* 12, no. 21 (2020): 11333–11363, <https://doi.org/10.1039/d0nr00732c>.
- [49] T. Liou, L. Hung, C. Liu, and T. Zhang, "Direct Synthesis of Nano Titania on Highly-Ordered Mesoporous SBA-15 Framework for Enhancing Adsorption and Photocatalytic Activity," *Journal of Porous Materials* 25, no. 5 (2018): 1337–1347, <https://doi.org/10.1007/s10934-017-0544-5>.
- [50] Q. Liu and Y. Tian, "One-Pot Synthesis of NiO/SBA-15 Monolith Catalyst With a Three-Dimensional Framework for CO₂ Methanation," *International Journal of Hydrogen Energy* 42, no. 17 (2017): 12295–12300, <https://doi.org/10.1016/j.ijhydene.2017.02.070>.
- [51] T. M. Diez-Rodríguez, E. Blázquez-Blázquez, E. Pérez, and M. Cerrada, "Composites Based on Poly (Lactic Acid)(pla) and Sba-15: Effect of Mesoporous Silica on Thermal Stability and on Isothermal Crystallization From Either Glass or Molten State," *Polymers* 12, no. 11 (2020): 2743, <https://doi.org/10.3390/polym12112743>.
- [52] T. Barbosa, T. Barros, T. L. Barbosa, and M. Rodrigues, "Green Synthesis for MCM-41 and SBA-15 Silica Using the Waste Mother Liqueur," *Silicon* 14, no. 11 (2022): 6233–6243, <https://doi.org/10.1007/s12633-021-01329-4>.
- [53] G. Medeiros de Paula, L. do Nascimento Rocha de Paula, and M. Freire Rodrigues, "Production of MCM-41 and SBA-15 Hybrid Silicas From Industrial Waste," *Silicon* 14, no. 2 (2022): 439–447, <https://doi.org/10.1007/s12633-020-00831-5>.
- [54] S. Mondal, S. Ruidas, S. Chongdar, B. Saha, and A. Bhaumik, "Sustainable Porous Heterogeneous Catalysts for the Conversion of Biomass Into Renewable Energy Products," *ACS*

- Sustainable Resource Management* 1, no. 8 (2024): 1672–1704, <https://doi.org/10.1021/acssusresmg.4c00190>.
- [55] N. Missaoui, A. Chrouda, F. Bourguiba, and J. Serafin, “Impact of Metal Precursor and Molar Ratios on Adsorption and Separation of CO₂ and CH₄ by SOD-ZIF-67 Prepared Using Green Solvent-Free Synthesis,” *Fuel* 378 (2024): 132840, <https://doi.org/10.1016/j.fuel.2024.132840>.
- [56] F. Silva, E. Rigoti, M. Mello, and S. Pergher, “Tuning Textural Properties by Changing the Morphology of SBA-15 Mesoporous Materials,” *Materials* 17, no. 12 (2024): 2827, <https://doi.org/10.3390/ma17122827>.
- [57] P. Jeyakumar, S. Thanikaikarasn, B. Natarajan, et al., “Synthesis and Functionalization of L, DL-Iso, Nor, Leucine on Porous Silicon for Sensing Application,” *Journal of New Materials for Electrochemical Systems* 18, no. 4 (2015): 237–241, <https://doi.org/10.14447/jnmes.v18i4.354>.
- [58] S. A. Selim, S. Hanafi, M. Abd-El-Khalik, and M. Ismail, “Thermal and Textural Characteristics of Modified Silica,” *Journal of Chemical Technology and Biotechnology-Chemical Technology* 35, no. 6 (1985): 297–307, <https://doi.org/10.1002/jctb.5040350606>.
- [59] F. Hassanzadeh-Afruzi, S. Asgharnasl, S. Mehraeen, Z. Amiri-Khamakani, and A. Maleki, “Guanidinylated SBA-15/Fe₃O₄ Mesoporous Nanocomposite as an Efficient Catalyst for the Synthesis of Pyranopyrazole Derivatives,” *Scientific Reports* 11, no. 1 (2021): 19852, <https://doi.org/10.1038/s41598-021-99120-3>.
- [60] N. Seroka, R. Taziwa, and L. Khotseng, “Green Synthesis of Crystalline Silica From Sugarcane Bagasse Ash: Physico-Chemical Properties,” *Nanomaterials* 12, no. 13 (2022): 2184, <https://doi.org/10.3390/nano12132184>.
- [61] J. Zhang, S. Yang, W. Cai, et al., “Efficient Production of Medium-Chain Structured Phospholipids Over Mesoporous Organosulfonic Acid-Functionalized SBA-15 Catalysts,” *Catalysts* 9, no. 9 (2019): 770, <https://doi.org/10.3390/catal9090770>.
- [62] V. Chaudhary and Sweta, “Synthesis and Catalytic Activity of SBA-15 Supported Catalysts for Styrene Oxidation,” *Chinese Journal of Chemical Engineering* 26, no. 6 (2018): 1300–1306, <https://doi.org/10.1016/j.cjche.2018.01.025>.
- [63] R. Subagyono, S. Putri, M. Manawan, M. Mollah, R. Nugroho, and R. Gunawan, “Catalytic Pyrolysis of the Green Microalgae Botryococcus Braunii Over Ni/SBA-15 Prepared by the Ultrasonic-Assisted Sol-Gel Method,” *ACS Omega* 8, no. 9 (2023): 8582–8595, <https://doi.org/10.1021/acsomega.2c07748>.
- [64] A. Sayari and Y. Yang, “SBA-15 Templated Mesoporous Carbon: New Insights Into the SBA-15 Pore Structure,” *Chemistry of Materials* 17, no. 24 (2005): 6108–6113, <https://doi.org/10.1021/cm050960q>.
- [65] A. Maria Chong and X. Zhao, “Functionalization of SBA-15 With APTES and Characterization of Functionalized Materials,” *The Journal of Physical Chemistry B* 107, no. 46 (2003): 12650–12657, <https://doi.org/10.1021/jp035877%2b>.
- [66] M. Ferdousi, M. Pazouki, F. Hessari, and M. Kazemzad, “Simultaneous Control of Rod Length and Pore Diameter of SBA-15 for PPL Loading,” *Journal of Porous Materials* 23, no. 2 (2016): 453–463, <https://doi.org/10.1007/s10934-015-0099-2>.
- [67] Q. Khanh Nguyen, N. Yen, N. Hau, and H. Tran, “Synthesis and Characterization of Mesoporous Silica SBA-15 and ZnO/SBA-15 Photocatalytic Materials From the Ash of Brick-yards,” *Journal of Chemistry* 2020, no. 1 (2020): 1–8, <https://doi.org/10.1155/2020/8456194>.
- [68] F. Farirai, M. Mupa, and M. Daramola, “An Improved Method for the Production of High Purity Silica From Sugarcane Bagasse Ash Obtained From a Bioethanol Plant Boiler,” *Particulate Science and Technology* 39, no. 2 (2021): 252–259, <https://doi.org/10.1080/02726351.2020.1734700>.
- [69] N. Ali, Z. Alismaeel, H. Majidi, et al., “RETRACTED: Modification of SBA-15 Mesoporous Silica as an Active Heterogeneous Catalyst for the Hydroisomerization and Hydrocracking of N-Heptane,” *Heliyon* 8, no. 6 (2022): e09737, <https://doi.org/10.1016/j.heliyon.2022.e09737>.
- [70] S. Ruthstein, J. Schmidt, E. Kesselman, Y. Talmon, and D. Goldfarb, “Resolving Intermediate Solution Structures During the Formation of Mesoporous SBA-15,” *Journal of the American Chemical Society* 128, no. 10 (2006): 3366–3374, <https://doi.org/10.1021/ja0559911>.
- [71] T. Benamor, L. Vidal, B. Lebeau, and C. Marichal, “Influence of Synthesis Parameters on the Physico-Chemical Characteristics of SBA-15 Type Ordered Mesoporous Silica,” *Microporous and Mesoporous Materials* 153 (2012): 100–114, <https://doi.org/10.1016/j.micromeso.2011.12.016>.
- [72] L. Xu, J. Zhang, J. Ding, et al., “Pore Structure and Fractal Characteristics of Different Shale Lithofacies in the Dalong Formation in the Western Area of the Lower Yangtze Platform,” *Minerals* 10, no. 1 (2020): 72, <https://doi.org/10.3390/min10010072>.
- [73] N. García, E. Benito, J. Guzmán, P. Tiemblo, V. Morales, and R. A. García, “Functionalization of SBA-15 by an Acid-Catalyzed Approach: A Surface Characterization Study,” *Microporous and Mesoporous Materials* 106, no. 1-3 (2007): 129–139, <https://doi.org/10.1016/j.micromeso.2007.02.043>.
- [74] J. Thielemann, F. Girgsdies, R. Schlögl, and C. Hess, “Pore Structure and Surface Area of Silica SBA-15: Influence of Washing and Scale-Up,” *Beilstein Journal of Nanotechnology* 2, no. 1 (2011): 110–118, <https://doi.org/10.3762/bjnano.2.13>.
- [75] R. Fonseca-Correa, Y. Murillo-Acevedo, L. Giraldo-Gutiérrez, and J. Moreno-Piraján, “Microporous and Mesoporous Materials in Decontamination of Water Process,” *Microporous and Mesoporous Materials* 10 (2016): 64393.
- [76] M. Kruk, M. Jaroniec, C. Ko, and R. Ryoo, “Characterization of the Pore Structure of SBA-15,” *Chemistry of Materials* 12, no. 7 (2000): 1961–1968, <https://doi.org/10.1021/cm000164e>.
- [77] L. Freitas, I. Bravo, W. Macedo, and E. de Sousa, “Mesoporous Silica Materials Functionalized With Folic Acid: Preparation, Characterization and Release Profile Study With Methotrexate,” *Journal of Sol-Gel Science and Technology* 77, no. 1 (2016): 186–204, <https://doi.org/10.1007/s10971-015-3844-8>.
- [78] H. Le, K. Ho, T. Le, V. Nguyen, H. X. Le, and K. Nguyen, “Synthesis and Application of SBA-15-Supported CuO as an Efficient Catalyst for the Oxidative C (Sp²)-O Coupling Reaction,” in *IOP Conference Series: Earth and Environmental Science*, 947, no. 1 (IOP Publishing, 2021), 012033, <https://doi.org/10.1088/1755-1315/947/1/012033>.
- [79] G. Chandrasekar, M. Hartmann, and V. Murugesan, “Preparation of SBA-15 Extrudates: Evaluation of Textural and Mechanical Properties,” *Journal of Porous Materials* 16, no. 2 (2009): 175–183, <https://doi.org/10.1007/s10934-007-9182-7>.
- [80] N. Rahmat, N. Sadon, and M. Yusof, “Thermogravimetric Analysis (TGA) Profile at Different Calcination Conditions for Synthesis of PTES-SBA-15,” *American Journal of Applied Sciences* 14, no. 10 (2017): 938–944, <https://doi.org/10.3844/ajassp.2017.938.944>.
- [81] A. Torres, B. Fuentes, K. E. Rodríguez, A. Brito, and L. Díaz, “Analysis of the Content of Fatty Acid Methyl Esters in Biodiesel by Fourier-Transform Infrared Spectroscopy: Method and Comparison With Gas Chromatography,”

- Journal of the American Oil Chemists' Society* 97, no. 6 (2020): 651–661, <https://doi.org/10.1002/aocs.12350>.
- [82] M. Bradley, *Biodiesel (FAME) Analysis by FT-IR, Application Note: 51285* (Thermo Fischer Scientific, 2007).
- [83] E. Wembabazi, P. Mugisha, A. Ratibu, D. Wendo, J. Kyambadde, and P. Vuzi, "Spectroscopic Analysis of Heterogeneous Biocatalysts for Biodiesel Production From Expired Sunflower Cooking Oil," *Journal of Spectroscopy* 2015, no. 1 (2015): 1–8, <https://doi.org/10.1155/2015/714396>.
- [84] G. Poulenat, S. Sentenac, and Z. Mouloungui, "Fourier-Transform Infrared Spectra of Fatty Acid Salts—Kinetics of High-Oleic Sunflower Oil Saponification," *Journal of Surfactants and Detergents* 6, no. 4 (2003): 305–310, <https://doi.org/10.1007/s11743-003-0274-1>.
- [85] L. Maina, *Rapid Identification of Edible Oils Manufactured in Kenya* (University of Nairobi, 2016).
- [86] S. Ngomade, C. Fotsop, K. Nguena, et al., "Catalytic Performances of CeO₂@ SBA-15 as Nanostructured Material for Biodiesel Production From Podocarpus Falcatus Oil," *Chemical Engineering Research and Design* 194 (2023): 789–800, <https://doi.org/10.1016/j.cherd.2023.05.010>.
- [87] H. Venkatesan, G. John, and S. Sivamani, "Cotton Seed Biodiesel as Alternative Fuel: Production and Its Characterization Analysis Using Spectroscopic Studies," *International Journal of Renewable Energy Resources* 7, no. 3 (2017): 1333–1339.
- [88] T. Morgan, E. Santillan-Jimenez, K. Huff, K. R. Javed, and M. Crocker, "Use of Dual Detection in the Gas Chromatographic Analysis of Oleaginous Biomass Feeds and Biofuel Products to Enable Accurate Simulated Distillation and Lipid Profiling," *Energy and Fuels* 31, no. 9 (2017): 9498–9506, <https://doi.org/10.1021/acs.energyfuels.7b01445>.
- [89] K. Hundie, L. Shumi, and T. Bullo, "Investigation of Biodiesel Production Parameters by Transesterification of Watermelon Waste Oil Using Definitive Screening Design and Produced Biodiesel Characterization," *South African Journal of Chemical Engineering* 41 (2022): 140–149, <https://doi.org/10.1016/j.sajce.2022.06.002>.
- [90] J. Figueiredo, B. Alves, V. Freire, J. Alves, and B. Barbosa, "Preparation, Characterization and Evaluation of X-MoO₃/Al-SBA-15 Catalysts for Biodiesel Production," *Materials for Renewable and Sustainable Energy* 11, no. 1 (2022): 17–31, <https://doi.org/10.1007/s40243-021-00204-x>.
- [91] L. Kathumbi, P. Home, J. Raude, and B. Gathitu, "Performance of Citric Acid as a Catalyst and Support Catalyst When Synthesized With NaOH and CaO in Transesterification of Biodiesel From Black Soldier Fly Larvae Fed on Kitchen Waste," *Fuel* 3, no. 2 (2022): 295–315, <https://doi.org/10.3390/fuels3020018>.
- [92] M. A. Zayed, M. Sm Abd El-Kareem, and N. Zaky, "Gas Chromatography-Mass Spectrometry Studies of Waste Vegetable Mixed and Pure Used Oils and Its Biodiesel Products," *Journal of Pharmaceutical and Applied Chemistry* 2, no. 1 (2016): 30–37.
- [93] E. Muzenda and J. Scheepers, "Influence of Temperature on Volatile Organic Compounds-Ester Solvent Interactions," *South African Journal of Chemical Engineering* 19, no. 2 (2014): 1–17.
- [94] P. Sahoo and L. Das, "Process Optimization for Biodiesel Production From Jatropha, Karanja and Polanga Oils," *Fuel* 88, no. 9 (2009): 1588–1594, <https://doi.org/10.1016/j.fuel.2009.02.016>.
- [95] H. Ghaedi and M. Zhao, "Review on Template Removal Techniques for Synthesis of Mesoporous Silica Materials," *Energy and Fuels* 36, no. 5 (2022): 2424–2446, <https://doi.org/10.1021/acs.energyfuels.1c04435>.
- [96] Q. Gao, W. Xu, Y. Xu, et al., "Amino Acid Adsorption on Mesoporous Materials: Influence of Types of Amino Acids, Modification of Mesoporous Materials, and Solution Conditions," *The Journal of Physical Chemistry B* 112, no. 7 (2008): 2261–2267, <https://doi.org/10.1021/jp0763580>.
- [97] E. S. Sanz-Pérez, M. Olivares-Marin, A. Arencibia, R. Sanz, G. Calleja, and M. M. Maroto-Valer, "CO₂ Adsorption Performance of Amino-Functionalized SBA-15 Under Post-Combustion Conditions," *International Journal of Greenhouse Gas Control* 17 (2013): 366–375, <https://doi.org/10.1016/j.ijggc.2013.05.011>.